Chem Soc Rev

REVIEW ARTICLE

View Article Online
View Journal | View Issue



Cite this: *Chem. Soc. Rev.*, 2016, 45, 5925

# Electrochemical capacitors: mechanism, materials, systems, characterization and applications

Yonggang Wang, Yanfang Song and Yongyao Xia*

Electrochemical capacitors (*i.e.* supercapacitors) include electrochemical double-layer capacitors that depend on the charge storage of ion adsorption and pseudo-capacitors that are based on charge storage involving fast surface redox reactions. The energy storage capacities of supercapacitors are several orders of magnitude higher than those of conventional dielectric capacitors, but are much lower than those of secondary batteries. They typically have high power density, long cyclic stability and high safety, and thus can be considered as an alternative or complement to rechargeable batteries in applications that require high power delivery or fast energy harvesting. This article reviews the latest progress in supercapacitors in charge storage mechanisms, electrode materials, electrolyte materials, systems, characterization methods, and applications. In particular, the newly developed charge storage mechanism for intercalative pseudocapacitive behaviour, which bridges the gap between battery behaviour and conventional pseudocapacitive behaviour, is also clarified for comparison. Finally, the prospects and challenges associated with supercapacitors in practical applications are also discussed.

Received 24th July 2015

DOI: 10.1039/c5cs00580a

www.rsc.org/chemsocrev

## 1. Introduction

Owing to the limited crude oil storage and global warming situation, there is an increasing need for a breakthrough in rechargeable batteries and/or supercapacitor science and technology to satisfy the future development of a low-carbon and sustainable economy.[1–5] Rechargeable batteries are being considered as promising power devices for electric vehicles (EVs) and efficient energy storage devices for sustainable energy, such as wind or solar energy.[1–3] However, the charge storage of current rechargeable batteries (*e.g.* aqueous Ni–MH batteries and non-aqueous Li-ion batteries) mainly depends on the intercalation/de-intercalation of cations ($H^+$ or $Li^+$) within the crystalline structure of electrode materials, and thus is controlled by the diffusion of cations within the crystalline framework, which significantly limits the charge/discharge rate (or power density) of batteries.[1–3] Supercapacitors, including electrochemical double-layer capacitors (EDLCs) and pseudocapacitors, can provide much greater power density than batteries because their charge storage is

*Department of Chemistry and Shanghai Key Laboratory of Molecular Catalysis and Innovative Materials, Institute of New Energy, iChEM (Collaborative Innovation Center of Chemistry for Energy Materials), Fudan University, Shanghai, 200433, China. E-mail: yyxia@fudan.edu.cn*

**Yonggang Wang**

*Yonggang Wang received his PhD in Physical Chemistry from Fudan University in 2007. From 2007 to 2011, he worked as a Post-doctoral Research Associate at the National Institute of Advanced Industrial Science and Technology (AIST), Japan. He is currently a full professor at the Department of Chemistry at Fudan University, China. His research interests include electrochemical functional materials and their application in lithium-ion batteries, metal–air batteries, supercapacitors, and fuel cells.*

**Yanfang Song**

*Yanfang Song received her PhD degree at Fudan University in June 2016, and BS degree at the School of Chemistry and Chemicals, from Fuzhou University, China in 2011. She is currently working as an assistant research fellow at Shanghai Advanced Research Institute, Chinese Academy of Sciences. Her research is focused on nanomaterials for energy conversion and storage.*

based on the surface reactions of electrode materials, without ion diffusion within the bulk of materials.[4–8] Accordingly, supercapacitors should be a promising alternative or complement to rechargeable batteries when high power delivery and/or fast energy harvesting are required. However, it should also be noted that the restriction of charge storage to the surface (or near-surface) of supercapacitors makes their capacity (or energy density) much lower than that of batteries. As a result, many efforts have been made to enhance their energy density.

It is well known that the energy density (E) of a supercapacitor depends on both the specific capacitance (F) of the electrode materials and the overall cell voltage (V). Accordingly, one efficient method is to develop porous and nano-sized electrode materials for improving capacitance. Another approach is to build hybrid/asymmetric supercapacitors, which can efficiently utilize the potential gap between the two types of electrodes to increase the overall cell voltage (V).

During the past years, many efforts have been made to develop nano-sized/nano-structured electrode materials to shorten the diffusion length and/or increase the outer surface area in order to improve the performance of rechargeable batteries or supercapacitors. Accordingly, some nano-sized/nano-structured battery-type electrode materials display a very fast charge/discharge rate, and many supercapacitor electrode materials exhibit much improved capacitance with an increased outer surface area.[3,5,9–12] Unfortunately, in this situation, many battery-type electrodes, such as $Ni(OH)_2$[13,14] or other materials, that exhibit faradaic behaviour (even those that are electrochemically irreversible)[15,16] have been considered as pseudocapacitive materials in many reports, which leads to confusion for readers. Even if the redox properties of battery materials are electrochemically reversible, they are much worse than those of pseudocapacitor materials. Battery materials with a poorer reversibility have a decreased energy efficiency, even though the columbic efficiency may be very high. Very recently, it has been demonstrated that several electrode materials display pseudocapacitive $Li^+$ intercalation, in which the charge storage within the crystalline framework of these materials is not controlled by the $Li^+$ diffusion process.[17–25] This phenomenon provides a new combined concept between the typical faradaic behaviour of battery-type electrodes and the pseudocapacitive behaviour of supercapacitor-type electrode, and thus may also result in further confusion. On the other hand, in recent years, some battery-type electrodes were coupled with supercapacitor-type electrodes to form hybrid supercapacitor systems with higher voltages and enhanced energy density, which also aggravates the confusion mentioned above. Especially, some researchers and/or readers may misconsider the ''hybrid'' supercapacitors systems as ''asymmetric'' supercapacitor systems that are based on two different supercapacitor-type electrodes (*i.e.* capacitive electrode and/or pseudocapacitive electrodes). As correctly pointed out by Brousse *et al.*,[26] the term ''hybrid'' supercapacitor should be used when pairing two electrodes with different charge storage behaviour, *i.e.*, one capacitive and one faradaic, and the performance of such a device is in-between a supercapacitor and a battery. An ''asymmetric'' supercapacitor covers a wider range of electrode combinations because it can be used for supercapacitors using two electrodes of the same nature but with different mass loadings, or two electrodes using different materials. Regarding the above confusion, Brousse *et al.* have given an excellent comment in their recent publication about the pseudocapacitive behaviour of supercapacitors.[26] Therefore, we do not include further discussion in this section.

As mentioned above, the main challenge for supercapacitors is to develop them with a high energy density that is close to that of current rechargeable batteries, while maintaining their inherent characteristics of high power and long cycling life. As a result, many researchers devoted efforts to enhancing their performance by either maximizing the specific capacitance (*i.e.* nano-sizing or nano-structuring capacitive and pseudocapacitive electrodes) and/or increasing the cell voltage (*i.e.* building asymmetric and hybrid supercapacitors). With these efforts, both the performance of supercapacitors and their corresponding applications are gradually improved, but there is also much confusion regarding the development process. As shown in Fig. 1, this article reviews the latest advances of supercapacitors in charge storage mechanisms, characterization methods, systems and related materials. Finally, the prospects and challenges associated with supercapacitors in practical applications are also discussed.

**Yongyao Xia**

*Yongyao Xia received his PhD degree in Energy-Related-Material Science at Saga University, Japan in 1997. In 1998, he worked at the Department of Chemical Engineering, University of South Carolina, as a Post-doctoral Research Associate. In 1999, he returned to Japan and worked as a Post-doctoral Research Associate in the Battery Section of Osaka National Research Institute. From 2001 to 2002, he worked as a Researcher at Hitachi Maxell Ltd Starting from 2003, he became a full professor at the Department of Chemistry at Fudan University, China. His research interests involve advanced materials and technologies for energy storage and conversion devices, e.g., lithium-ion batteries, electrochemical supercapacitors, and fuel cells. He serves as the editor of the Journal of Power Sources.*

## 2. Charge storage mechanism of supercapacitor

In this section, the charge storage mechanisms of supercapacitors (both EDLC and pseudo-capacitors) are compared with those in batteries and with intercalative pseudocapacitive behaviour. Also the most important issue of how to distinguish between a capacitive profile and a battery profile is discussed.

The capacity of current rechargeable batteries mainly depends on the intercalation/de-intercalation of cations ($H^+$ or $Li^+$) within

 

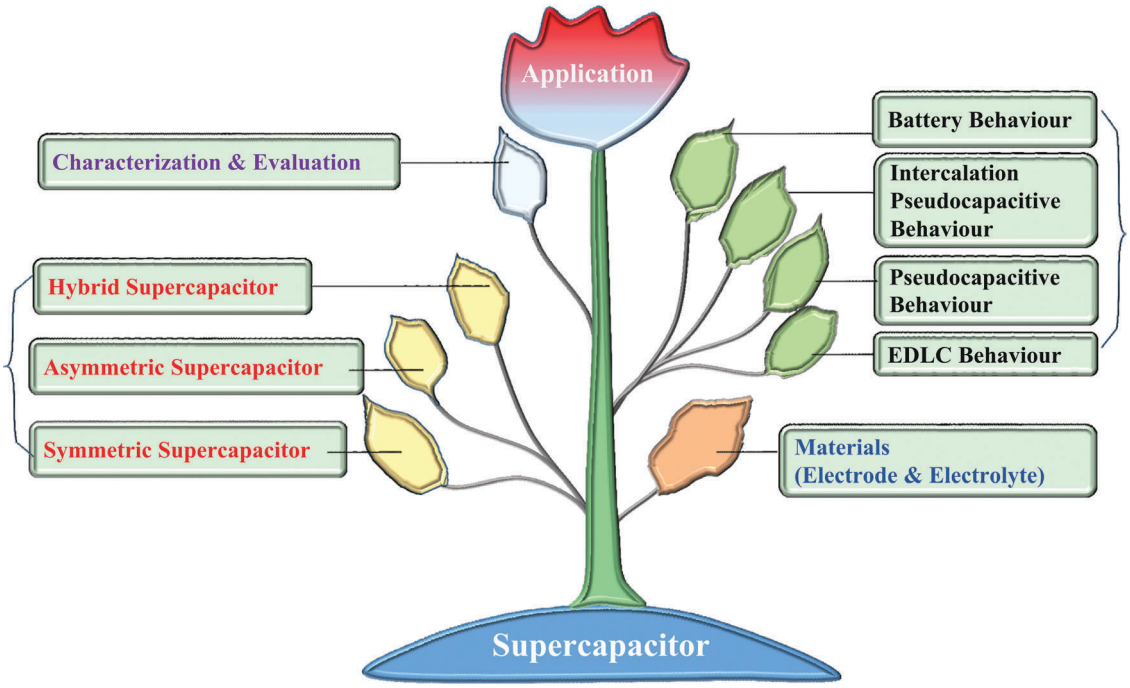


Fig. 1 Schematic of the current review content.

the crystalline structure of electrode materials, coupled with the redox reactions of metal ions within the crystalline structure (Fig. 2a). For example, in the charge process of aqueous Ni–MH batteries, a proton ($H^+$) is extracted (*i.e.* de-intercalated) from the crystalline framework of an $Ni(OH)_2$ cathode to form NiOOH.[27] On discharge, the proton is inserted into the crystalline framework to form $Ni(OH)_2$.[27] Obviously, the charge/discharge is coupled with redox of $Ni^{2+}/Ni^{3+}$ ions and electron gain/loss (Fig. 2a). Similarly, the charge/discharge of conventional Li-ion batteries depends on $Li^+$ intercalation/de-intercalation.[1–4] For instance, on the charging of an $LiCoO_2$–graphite battery, $Li^+$ is extracted from the crystalline framework of the $LiCoO_2$ cathode to form $CoO_2$. Its discharge reverses the charge process. As shown in Fig. 2a, the charge storage of a battery is controlled by cation diffusion within a crystalline framework. It should be noted that the mechanisms involved in all rechargeable batteries also involve "phase-transformation" and/or alloying reactions, besides the intercalation reaction mentioned above. Herein, we only employ the intercalation reaction in the Li-ion battery (or Ni–MH battery) as a typical example to clarify that the charge storage mechanism of a supercapacitor is different from that of a rechargeable battery.

The capacitance of supercapacitors mainly arises from surface reactions of electrode materials, including electrochemical adsorption/desorption of cations and anions at the electrode/electrolyte interface (*i.e.*, capacitive behaviour; Fig. 2b), and surface faradic redox reactions (*i.e.*, pseudocapacitive behaviour; Fig. 2b).[5–8] Accordingly, supercapacitors can be classed as: electrochemical double-layer capacitors (EDLCs) and pseudocapacitors.[5–8] In recent years, porous carbon has been widely used as the electrode material for EDLCs. Transition metal oxides or conductive polymers exhibit typical pseudocapacitance, and display much higher specific capacitance than carbon materials for EDLCs.[5–8]

As mentioned above, both rechargeable batteries and pseudocapacitors store charges *via* a redox reaction of the metal ions in electrode-active materials. Their difference is that the former is limited by cation diffusion within the crystalline framework of active material, while the latter is not controlled by the diffusion process. Cyclic voltammetry (CV) investigation is an efficient tool to clarify this kinetic difference. In theory, the voltammetric response of an electrode active material at various sweep rates can be summarized according to:[22,28,29]

$$i = av^b \quad (1)$$

in which the measured current ($i$) at a fixed potential obeys a power law relationship with the potential sweep rate ($v$). It has been clearly demonstrated that the intercalation of battery behaviour is controlled by cation diffusion in the crystalline framework of electrode materials, and the corresponding voltammetric response can be summarized as:[29]

$$i = nFAC^*D^{1/2}v^{1/2}(\alpha nF/RT)^{1/2}\pi^{1/2}\chi(bt) \quad (2)$$

where $C^*$ is the surface concentration of the electrode material, $\alpha$ is the transfer coefficient, $D$ is the chemical diffusion coefficient, $n$ is the number of electrons involved in the electrode reaction, $A$ is the surface area of the electrode material, $F$ is the Faraday constant, $R$ is the molar gas constant, $T$ is the temperature, and the function ($bt$) represents the normalized current. Accordingly, for battery behaviour, the relationship between the peak current ($i_p$) and the sweep rate ($v$) can be presented by $i_p = av^{0.5}$ ($b = 0.5$). In contrast to battery behaviour, typical capacitive behaviour or pseudocapacitive behaviour is not diffusion-controlled, and thus

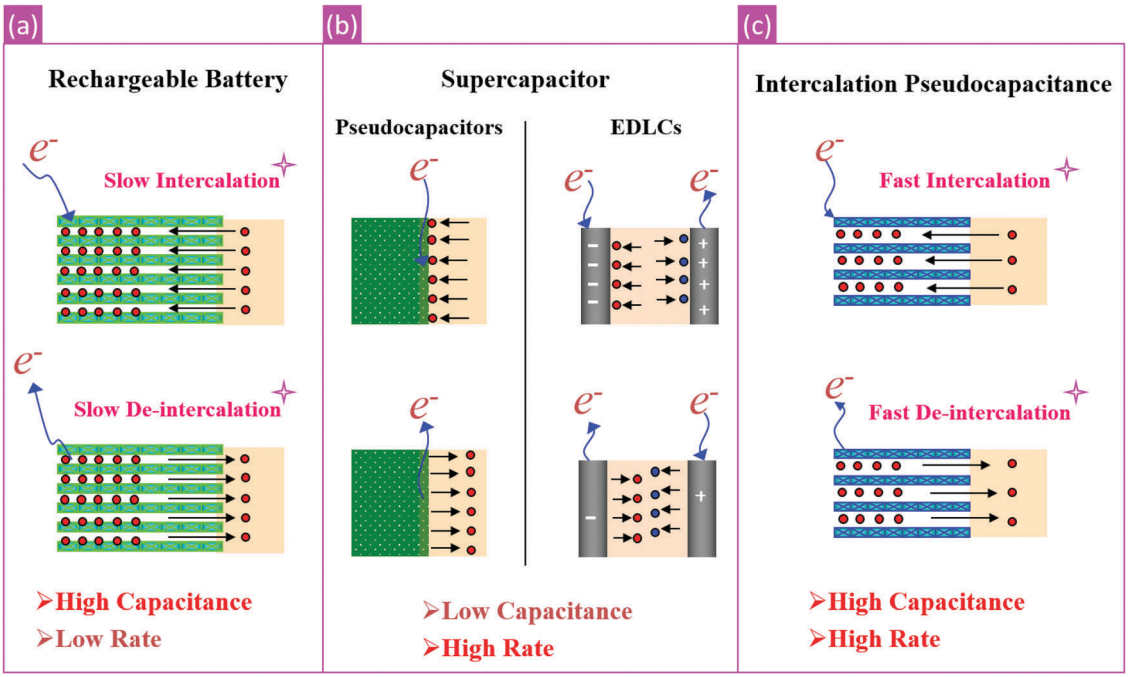


Fig. 2 Schematic of different charge storage mechanisms. (a) Charge storage mechanism of rechargeable battery. (b) Charge storage mechanism of supercapacitor. (c) Charge storage mechanism of intercalation pseudocapacitance.

the current ($i$) should vary linearly with the sweep rate ($b$ = 1) according to:[22,28,29]

$$i = C_d A v \quad (3)$$

where $C_d$ represents the capacitance and $A$ is the surface area of the active materials.[29]

In the pseudocapacitance case, the electrode potential associated with the electroadsorbed electroactive species is a continuous logarithmic function of the extent of sorption.[5–8] However, for most battery-type electrodes, the electrode potential is determined at some singular value by the Gibbs energies of pure, well-defined phases and usually also the composition and/or concentration of the solution.[26,30] Therefore, a pseudocapacitive electrode generally displays a linear dependence of the charge stored with the charging potential within the window of interest, but in which charge storage originates from electron-transfer mechanisms, rather than simply relying on the accumulation of ions in the electrochemical double layer (as with activated carbons). On the contrary, the charge storage of a battery-type electrode generally occurs in the special potential, and thus there are typical plateaus in the charge/discharge curves of battery-type electrodes. This difference between pseudocapacitive behaviour and battery behaviour is more obvious and direct in the CV investigation. The former generally exhibits a rectangular CV shape that is close to that of the capacitive profile from carbon electrode materials, while the latter displays clear redox peaks in CV curves.

As a new type of charge storage mechanism, intercalation pseudocapacitance depends on the intercalation/de-intercalation of cations (*e.g.* $Li^+$, $Na^+$, $K^+$, and $H^+$) in the bulk of active materials, but is not limited by the diffusion of cations within the crystalline framework of active materials (Fig. 2c). In cation-intercalated pseudocapacitance, the advantage of batteries (*i.e.* charge storage in the bulk of the electrode materials) is united with the advantage of supercapacitors (*i.e.* charge storage without diffusion control). Therefore, the peak current ($i_p$) for intercalation pseudocapacitive behaviour should also vary linearly with the sweep rate ($b$ = 1 or $i_p = C_d A v$). On the other hand, it was also found recently that, for some electrode materials, only part of the capacity arises from intercalation pseudocapacitance, but the intercalation pseudocapacitance contributes to a large portion of the overall capacity. For these materials, the relationship between the redox peak current ($i_p$) and the sweep rate ($v$) can also be summarized by eqn (1) (*i.e.* $i_p = a v^b$), but the $b$-value is only close to and slightly less than 1, which is different from the investigations mentioned above. In other words, these materials exhibit a hybrid charge storage mechanism, and their current response ($i$) at a fixed potential ($V$) can be described as the combination of two separate mechanisms, namely capacitive effects ($k_1 v$) and diffusion-controlled insertion ($k_2 v^{1/2}$) according to:[22]

$$i(v) = k_1 v + k_2 v^{1/2} \quad (4)$$

where $v$ is the sweep rate. By determining both $k_1$ and $k_2$, it is thus possible to distinguish the fraction of the current arising from cation intercalation and that from capacitive processes at specific potentials. It should also be noted that, although the kinetics ($b$) of intercalation pseudocapacitive behaviour is close to that of capacitive or conventional pseudocapacitive behaviour, its electrode profile is still similar to that of a battery-type electrode, in which charge storage occurs in a very narrow potential window.

 

# 3. Materials for supercapacitor

## 3.1 Carbon materials with capacitive behaviour

It is well known that carbon material is a type of prospective electrode material for supercapacitors (*i.e.* EDLCs), due to its abundance, easy processing, non-toxicity, high specific surface area, good electronic conductivity, high chemical stability, and wide operating temperature range.[31] Various carbon materials, including activated carbon, carbon nanotubes (CNTs), porous carbon, and graphene, have been widely reported as electrode materials for EDLCs over the past years. Carbon materials for EDLCs have been well reviewed recently;[32,33] herein, we briefly summarize the latest advances in the development of carbon materials for EDLCs. Recent developments mainly focus on porous structure optimization, morphology control, and surface modification.

As mentioned above, the conventional electrode materials for EDLCs are porous activated carbons (AC) with large specific surface areas of more than 2000 $m^2 g^{-1}$, which deliver capacitances of 200 F $g^{-1}$ and 100 F $g^{-1}$ in aqueous and organic electrolytes, respectively. Generally, the charge accumulation capability of carbon materials at the electrode/electrolyte interface is increased with their specific surface area (SSA).[34] However, specific capacitance is not always linearly increased because of the wide pore size distribution of activated carbon materials, which possess micropores (0.3 nm), macropores and random pore connections. These micropores, with a pore size less than 0.5 nm, are hardly accessible to electrolyte ions. Therefore, the ion transport in pore channels may dramatically slow down, and then the energy and power density of EDLCs will be limited, especially for organic systems.[35] Researchers have since developed another type of carbon material with a narrow distribution in the mesopore range (2–50 nm) and a uniform pore connection, that is, ordered mesoporous carbons (OMCs).[36] These OMCs overcome the drawback of conventional AC and exhibit a much better electrochemical performance, especially at high current densities, since the ordered mesopore channels and their interconnections benefit the penetration and transportation of organic electrolyte ions. For instance, CMK-3, prepared by a hard template (SBA-15) method, shows a fiber-like close stacking structure with a pore diameter of 3.90 nm and an SSA of 900 $m^2 g^{-1}$. When used as the electrode material for supercapacitors, CMK-3 delivers a specific capacitance of 90 F $g^{-1}$ in organic electrolytes.[36,37] In recent years, various OMCs have been developed and employed as electrode materials for EDLCs,[35–44] and this has been well reviewed recently.[45]

However, OMCs still have limited capacitance due to the porosity of their large mesopores and their relatively low surface area of approximately 1000 $m^2 g^{-1}$. Therefore, an appropriate pore size also plays a significant role in the capacitance enhancement of carbon materials. Recently, some researchers reported that the highest capacitances could be obtained when the pore size matches the radius of the electrolyte ions.[46,47] Gogotsi *et al.* have reported an anomalous increase in capacitance for carbide-derived carbons (CDCs) when their pore sizes are below 1 nm,[48] which suggests that charge storage in pores smaller than the diameters of solvated electrolyte ions (<1 nm) will achieve high capacitance (Fig. 3). The micropores (<1 nm) of the CDCs could increase the specific capacitance, and the uniform mesopores of ordered mesoporous carbon could lead to a high rate capability. Considering both of these, Liu *et al.*[35] developed a type of ordered hierarchical mesoporous/microporous carbon (OHMMC) by *in situ* chlorination of carbides in prepared ordered mesoporous nanocrystalline titanium carbide/carbon composites. The obtained OHMMCs possess a 2D hexagonal mesostructure (*p6m*), including a narrow mesopore size at 3.0 nm and micropores (0.69 and 1.25 nm) on the mesopore walls. As shown in Fig. 4a, the ordered mesoporous channels benefit the electrolyte immersion and retention, providing a more favorable path for the electrolyte. Meanwhile, the increased specific surface area arising from the micropores on the mesopore walls can provide more sites for charge storage. This unique ordered hierarchical porous structure allows it to deliver a high capacitance of 146 F $g^{-1}$ in organic electrolytes, maintaining the perfect rectangular shapes of cyclic voltammetry curves and retaining a high specific capacitance, even at a high scan rate of 200 mV $s^{-1}$ (Fig. 4b).

Recently, Li and co-workers reported that a hierarchical porous carbon, using resol as the precursor and KOH as both the template and activating agent, exhibits a high surface area (up to 2700 $m^2 g^{-1}$) and well-interconnected macropores with micropores and mesopores decorated on the carbon walls.[49] Consequently, the as-prepared sample shows low internal resistance, high specific capacitance (307 F $g^{-1}$), an excellent rate performance and outstanding cycling stability in 6 M KOH as a supercapacitor electrode. Moreover, Sevilla *et al.* reported that the hierarchical microporous/mesoporous structure of a highly porous carbon nanosheet, prepared by carbonization of sodium gluconate, allows electrolyte ions to rapidly move throughout its carbonaceous matrix, delivering an excellent capacitive performance.[50] Therefore, even at an ultra-high current load of 150 A $g^{-1}$ in 1 M $H_2SO_4$ and 120 A $g^{-1}$ in 1 M $TEABF_4$/AN, the hierarchical nanosheets exhibit specific capacitances of up to 140 F $g^{-1}$ and 100 F $g^{-1}$, respectively.

As reported by Conway,[51] the carbons used as the electrode materials of double-layer-type supercapacitors must have three properties: high specific surface areas of more than 1000 $m^2 g^{-1}$, good intra- and inter-particle conductivity, and outstanding electrolyte accessibility to the intra-pore space of the carbon materials. As mentioned above, a hierarchical porous structure can allow the advanced performance of supercapacitors due to the following two factors: abundant micropores and mesopores can provide a large accessible surface area, leading to a large capacitance and high energy density, while interconnected mesopores and macropores facilitate ion transport into the intra-pore space of carbon materials, which ensures high rate capability and high power density. According to the second property suggested by Conway, the morphologies and composites should also be considered in the process of selecting supercapacitor electrode materials.

Because of the inherent high electrical conductivity and chemical stability, carbon nanotubes (CNTs) have been considered as promising electrodes for supercapacitors.[52] However, the low surface area gives the capacitance of CNTs a limited value of

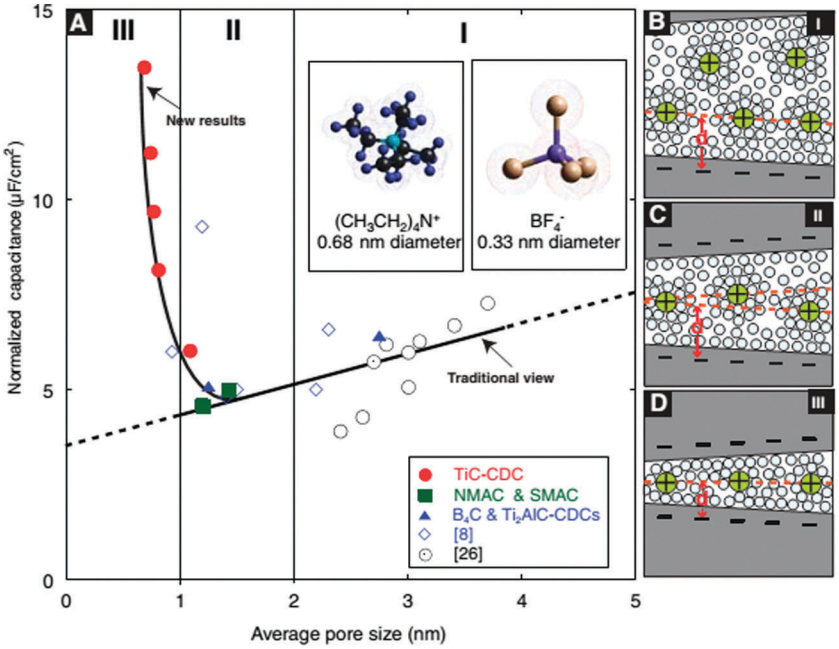


Fig. 3 (A) Plot of specific capacitance normalized by BET SSA and average pore size for carbons; Drawings of solvated ions residing in pores with the distance between adjacent pore walls: (B) greater than 2 nm, (C) between 1 and 2 nm, and (D) less than 1 nm, to illustrate distinguishing behaviour schematically. (Reproduced from ref. 48, with permission from the American Association for the Advancement of Science.)

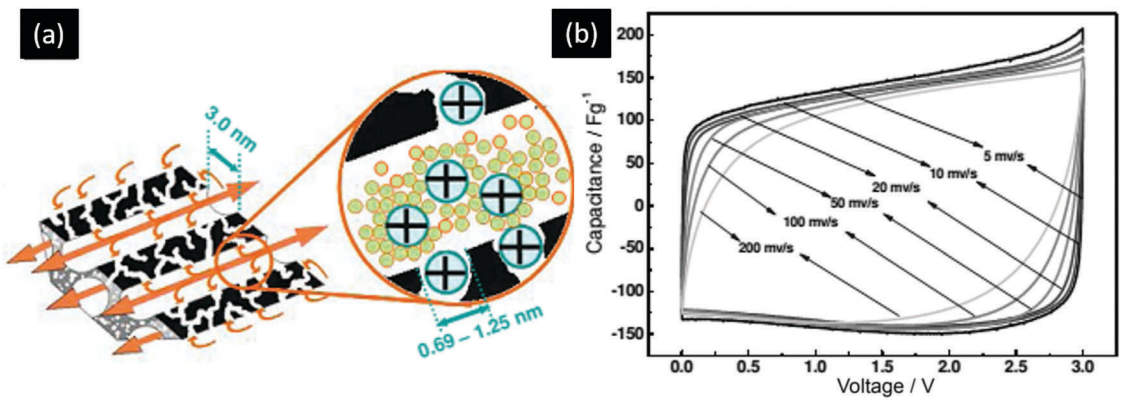


Fig. 4 (a) Schematic of the porous structure characteristic and the electrochemical reaction process of OHMMC and (b) CV curves of OHMMC at different scan rates. (Reproduced from ref. 35, with permission from John Wiley & Sons.)

about 30 F $g^{-1}$ in organic electrolytes.[53] Accordingly, various approaches have been used to increase the surface area of CNTs by treatment with acids/bases or by preparing densely packed CNT arrays.[54,55] For example, an SWNT-based macroscopic bulk form, reported by Futaba *et al.*, exhibits a high surface area of 1000 $m^2$ $g^{-1}$ and a capacity of 80 F $g^{-1}$ in organic electrolytes.[55] As a typical 2-D material with high electrical conductivity and charge transport mobility,[56] graphene is attracting extensive attention as an electrode material for high-power EDLCs. For example, Miller *et al.*[57] reported that graphene nanosheets grown on a metal current collector exhibited a high power performance that is even close to that of conventional dielectric capacitors. Very recently, porous graphene oxide prepared by KOH activation was investigated as an electrode material for EDLCs.[58] It was demonstrated that its capacitance, calculated from CV tests, almost remained at a constant value of 160 F $g^{-1}$, with an increase in sweep rates from 100 mV $s^{-1}$ to 500 mV $s^{-1}$.[58] As another most important direction, mesoporous carbon materials have been designed with various morphologies in order to improve their electronic conductivity, including a well-aligned free-standing mesoporous carbon nanofiber,[42,59] mesoporous carbon nanotubes,[38] mesoporous carbon sphere arrays,[39,43,44] and mesoporous carbon nanofiber arrays.[39] Very recently, Liu and co-workers prepared highly ordered mesoporous carbon nanofiber arrays (MCNAs) by combining a surfactant-templating self-assembly of organic resol with a natural crab-shell-templating process, in which the crab shell is used as a hard-template for the generation of the nanofiber array (Fig. 5).[41] This shows a

 

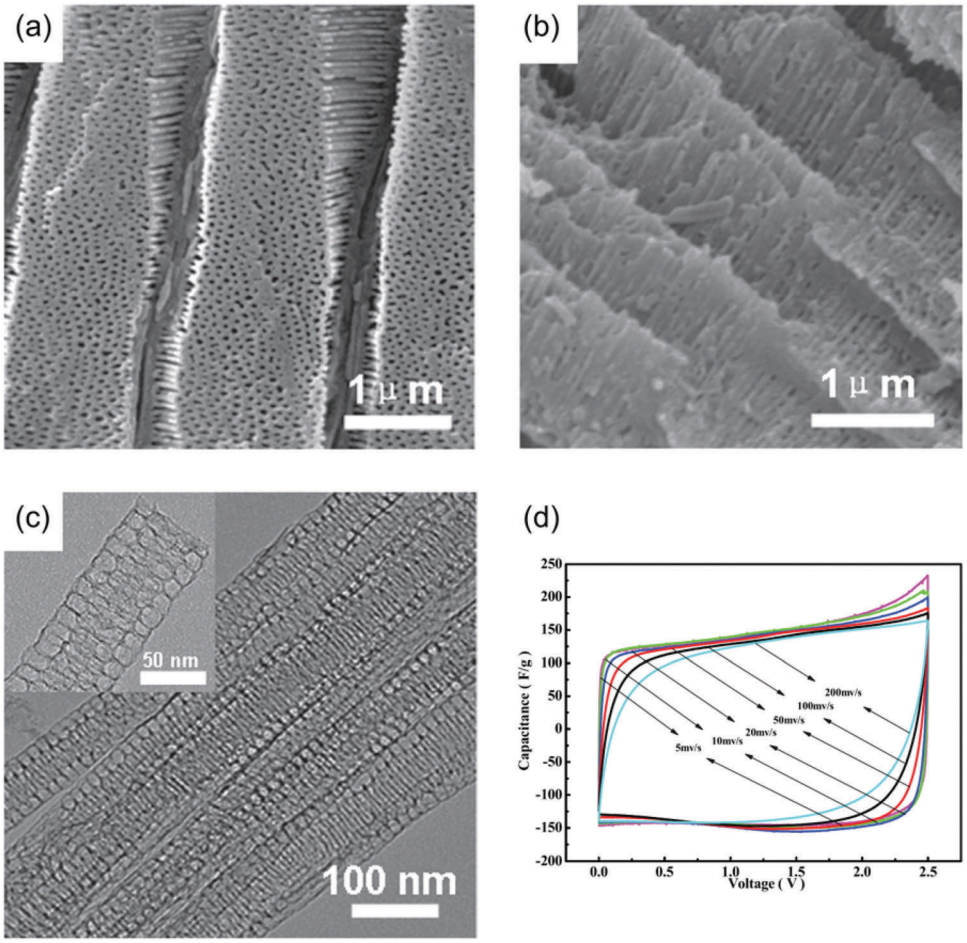


Fig. 5 (a) Side-view scanning electron microscopy (SEM) images obtained by vertically fixing one flat piece of crab shell on the conductive tape, (b) and (c) SEM/transmission electron microscopy (TEM) images, and (d) CV curves at various scan rates of the ordered mesoporous carbon nanofiber arrays prepared from the crab shell. (Reproduced from ref. 41, with permission from the Royal Society of Chemistry.)

high specific capacitance of 152 F $g^{-1}$, a high rate capability and excellent cycling ability. Also, some researchers exploited this to load the porous carbon on a highly electrically conductive support medium, such as CNT and graphene, to improve its capacitive profile. For instance, Zhao *et al.* synthesized CNT@mesoporous carbon with a core–shell configuration.[60] Liu and co-workers developed hierarchically porous composites with interconnected macroporous graphene networks covered by OMC with a uniform pore size of 9.6 nm.[61] They also demonstrated that the orientation of the mesopores (vertical or horizontal to the surface of the composites) can be tuned by the ratio of the components, which further influences the electrochemical behaviour of the composites. When used as the electrode material for supercapacitors in 6 M KOH electrolyte, the OMC/graphene with vertical mesopores exhibits an outstanding specific capacitance of 197 F $g^{-1}$ at a current density of 0.5 A $g^{-1}$.

In addition to a high specific surface area, an appropriate pore size and electrical conductivity, surface functionalization is another effective approach to improve the capacitive performance of carbon materials. The most popular heteroatoms introduced into the carbon frameworks are nitrogen, oxygen, boron and sulfur. Among these, nitrogen-containing carbon materials have been widely investigated as electrode materials for supercapacitors. Since the nitrogen-containing groups can generate or increase redox reactions, electron donor capability, and electrode wettability, incorporating nitrogen in carbon materials can greatly improve the capacitive performance.[62] Very recently, Zhou and co-workers developed a type of nitrogen-enriched ordered mesoporous carbon nanofiber array, which possesses a high specific surface area of 1030 $m^2$ $g^{-1}$, uniform mesopores located at 15.0 nm and a high nitrogen content of 6.7 wt%. These outstanding structural properties give it a high capacitance of 264 F $g^{-1}$ in supercapacitors.[63] By further increasing the surface area or modifying the pore size, a capacitance as large as 325 F $g^{-1}$ was achieved for these nitrogen-doped carbon materials.[64,65] In the carbons, nitrogen atoms can normally be classified into three different types: pyridinic-type nitrogen, which is $sp^2$ bonded to two carbon atoms and donates one p electron to the aromatic system; pyrrolic-type nitrogen, which is associated with a phenolic or carbonyl group on the neighboring carbon atom of the five-membered ring; and quaternary-type nitrogen, which is bonded to three carbon atoms in the central or the valley position of

graphene layers.[66] Those groups with nitrogen located at the edges of graphene layers, such as pyridinic-type nitrogen and pyrrolic-type nitrogen, are considered to introduce a pseudocapacitance effect, whereas quaternary-type nitrogen carrying positive charges can promote electron transfer through the carbon.[67] Additionally, oxygen is another promising heteroatom that has been widely researched to modify the surface of carbon materials. As for oxygen atoms in the carbons, they can also be divided into three different types: C=O quinone-type oxygen, C–OH phenol groups and/or C–O–C ether groups, and COOH chemisorbed oxygen and/or water. It is noted that only quinine-type oxygen is electrochemically active in acidic electrolytes. For example, Zhao and co-workers developed a hierarchical porous carbon with abundant oxygen functional groups produced by $HNO_3$ activation.[68] The abundant oxygen functional groups contribute stable pseudocapacitance and give the as-prepared sample a high specific capacitance (369 F $g^{-1}$ in 1 M $H_2SO_4$). Generally, nitrogen and oxygen are always co-doped into the carbon frameworks due to their synergistic effect. For instance, Li and co-workers fabricated a nitrogen- and oxygen-enriched hierarchical porous carbon fiber by phase-separable wet spinning and subsequent chemical activation of polyacrylonitrile (PAN) precursors.[69] The prepared carbon fiber possesses a high specific surface area of 2176 $m^2$ $g^{-1}$ and delivers a highly reversible specific capacitance of 329 F $g^{-1}$ at 0.1 A $g^{-1}$ in a two-electrode supercapacitor. As mentioned above, the presence of nitrogen and oxygen functional groups on the surface of carbon materials can induce faradaic redox reactions, which can be observed on its CV curves. As shown in Fig. 6, the current increase at potentials below 0.2 V on the CV curve of N-doped mesoporous carbon can be ascribed to the faradaic reactions of pyridinic-type nitrogen and pyrrolic-type nitrogen, while the redox humps between 0.2 and 0.4 V on the CV curves may be attributed to the pseudo-capacitance of quinone-type oxygen.

The synthesis processes mentioned above, such as hard-template or soft-template methods, are so complicated that a simpler approach is needed. Recently, a simple biomass carbonization method has been widely investigated because it does not require any chemical agents, since only a carbonization process is needed. Additionally, biomass sources are abundant, low cost, widely available and environmentally friendly. Moreover, the pore structure of the resultant carbons after carbonization is largely dependent on the biomass precursor. Thus, porous carbons with controlled microstructures that are also doped with the required heteroatoms can be obtained by carbonization of a selected biomass precursor. For example, Jin *et al.* fabricated carbon-based microporous nanoplates (CMNs), containing numerous nitrogen and oxygen atoms, from silk fibroin.[70] This type of CMN exhibits a high surface area of 2557 $m^2$ $g^{-1}$ and a high capacitance of 264 F $g^{-1}$ at a current density of 0.1 A $g^{-1}$ in 1 M $H_2SO_4$ electrolyte. Ogale and co-workers used yogurt to synthesize heavily nitrogen (12 wt%) doped porous carbon with a surface area of 1300 $m^2$ $g^{-1}$ and a capacitance of 225 F $g^{-1}$ at 2 A $g^{-1}$ in 1 M $H_2SO_4$ electrolyte.[71] Fan's group synthesized three-dimensional interconnected honeycomb-like porous carbon (HPC) foam by a one-step carbonization of alkali-treated wheat flour.[72] The interconnected porous structure, high specific surface area (1313 $m^2$ $g^{-1}$) and heteroatom doping (N: 1.1 at%, O: 11.2 at%) cause the HPC electrode to exhibit a high specific capacitance of 473 F $g^{-1}$ at 0.5 A $g^{-1}$ in 6 M KOH electrolyte. Eggplant, due to its sheet-like microstructure and nitrogen content, was chosen by Yang *et al.* to prepare nitrogen-doped porous carbon sheet.[73]

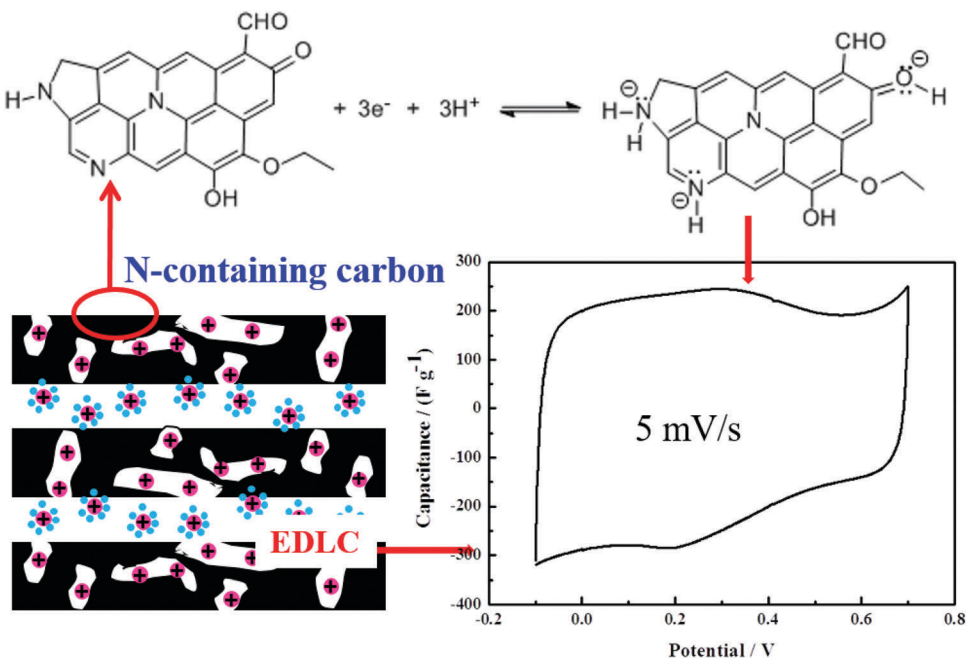


Fig. 6 Schematic of the electrochemical reaction of nitrogen-containing and oxygen-containing functional groups in the mesoporous carbons and its contribution to the capacitance enhancement on CV curves. (Reproduced from ref. 64, with permission from John Wiley & Sons.)

 

### 3.2 Metal oxides with pseudocapacitive behaviour

It is well known that the pseudocapacitance of metal oxides arises from both faradic redox reactions and the electrochemical adsorption/desorption of ions at the electrode/electrolyte interface. Therefore, metal oxides generally have much higher special capacitance compared with that of carbon materials for EDLCs. As summarized in Section 2, both battery-type electrodes and pseudocapacitive electrodes involve reactions requiring faradaic charge transfer. However, their kinetics and electrochemical profiles are totally different. During the past years, various metal oxides (*e.g.* $RuO_2{\cdot}H_2O$, $IrO_2{\cdot}H_2O$, $MnO_2{\cdot}H_2O$, $V_2O_5$, NiO, $Co_3O_4$, $SnO_2$, and $Fe_2O_3$) and some hydroxides (such as $Co(OH)_2$, $Ni(OH)_2$, or their composites) have been widely investigated as pseudocapacitive electrode materials.[74,75] Zhang *et al.*'s recent review article has given an excellent summary of these pseudocapacitive electrode materials.[32] Very recently, Thierry *et al.* presented a different opinion about a previous investigation on pseudocapacitive electrode materials.[26] They correctly pointed out that $Ni(OH)_2$, which is the electrode material of commercial Ni–MH or Ni–Cd batteries, cannot be considered as a pseudocapacitive electrode material. It is also undoubted that both the kinetics and electrochemical profile of $Ni(OH)_2$ exhibit the typical characteristics of a battery-type electrode, although there are many papers that describe $Ni(OH)_2$ as pseudocapacitive. In addition, Thierry *et al.* also claim that other Ni-based or Co-based electrodes cannot be described as pseudocapacitive electrode materials, because their electrochemical profile does not follow Conway's original definition of the term, pseudocapacitance. Owing to recent review articles, it is not necessary to further list the progress on pseudocapacitive electrode materials in detail. Therefore, we just give a brief review of the development of pseudocapacitive electrode materials, with further discussion on Thierry *et al.*'s comment. By reviewing previous investigations on pseudocapacitive materials, we find that the development mainly involves three categories, *i.e.* (1) Ru-based materials, (2) Mn-based materials, and (3) Ni or Co-based materials, which are summarized as follows.

It is well known that Conway *et al.*,[7] in collaboration with Craig of Continental Group, Inc., first studied the charge storage performance of $RuO_2$ in 1975. Then, the concept of a supercapacitor was introduced. Conway *et al.*'s investigation indicates that the redox processes involved in $RuO_2$-based materials require successive electron transfer at reaction centers ($Ru^{2+}$, $Ru^{3+}$, $Ru^{4+}$), while the proton transfer needed for conversion of $OH^-$ to $O^{2-}$ sites in the oxide structure can balance the electron transfer. In their report, the chemical and associated electrode potentials are a continuous function of the degree of charge, which was different from the thermodynamic behaviour of battery reactants. Therefore, according to Conway *et al.*'s early reports, the pseudocapacitive behaviour for hydrous $RuO_2$ generally exhibits a rectangular CV shape that is close to that of the capacitive profile from carbon electrode materials, while typical battery behaviour displays clear redox peaks in CV curves. Using Kr desorption BET measurements of the dry material, they also demonstrated that the capacitance per gram of hydrous $RuO_2$ is about 10 times what could be accounted for by double-layer charging with $C_{dl}$ taken as *ca.* 40 F (real $cm^2$)$^{-1}$. A later investigation demonstrated that the charge storage of hydrous $RuO_2$ was not limited by ion diffusion within the crystalline framework, whereas the charge storage of battery-type electrodes was generally controlled by ion diffusion within the bulk of electrode-active materials. However, the impedance behaviour of a $RuO_2$-based supercapacitor is far from that expected for an electrostatic capacitor. In brief, Conway *et al.*'s investigation first provides examples of the transition between battery and supercapacitor (*i.e.* EDLCs at that time) behaviour, arising from a range of degrees of oxidation/reduction that arise over an appreciable range of potentials. Afterward, hydrous $RuO_2$ was widely considered as a supercapacitor (*i.e.* pseudocapacitor) electrode material. In 1995, Zheng *et al.*[76] first reported that hydrous $RuO_2$ can reach a specific capacitance of 720 F $g^{-1}$, and demonstrated that the charge storage mechanism involves bulk electrochemical protonation of the oxide. Furthermore, they also investigated pseudocapacitors made with hydrous $RuO_2$ and hydrogen-inserted hydrous $RuO_2$ (*i.e.* $H_xRuO_2{\cdot}xH_2O$), and concluded that the $H_xRuO_2{\cdot}xH_2O$-based pseudocapacitor displayed a higher electrochemical performance.[77] In 2003, layered ruthenic acid (*i.e.* $H_xRuO_{2+y}{\cdot}zH_2O$), which has an expandable interlayer and can be delaminated into colloidal ruthenic acid nanosheets, was reported by Sugimoto *et al.*[78] as a promising electrode material for electrochemical supercapacitors that can provide high energy density even at high-power specifications. In their CV investigation, the current ($i$) linearly increases from 2 mV $s^{-1}$ to 500 mV $s^{-1}$, indicating much higher electrode kinetics than a conventional battery-type electrode. Since then, it has attracted extensive attention to increase the utilization of Ru.[77,79–84] For example, Hu *et al.*[85] achieved the maximal utilization of $RuO_x{\cdot}nH_2O$ (1340 F $g^{-1}$ measured at 25 mV $s^{-1}$) by a combined improvement in proton exchange and electronic conductivity of the electrode materials during the charge storage/delivery processes. As summarized in Zhang *et al.*'s review article,[32] many studies have also focused on combining $RuO_2$ with cheap metal oxides, such as $SnO_2$, $MnO_2$, NiO, $VO_x$, $TiO_2$, $MoO_3$, $WO_3$, and CaO, to form composite oxide electrodes.[86–89]

Despite the remarkable performance of this material, the high cost and environmental harmfulness exclude Ru-based electrode materials from wide application in supercapacitors. As an alternative approach, significant efforts have been devoted to developing low-cost and environmentally friendly materials that present electrochemical behaviour similar to that of $RuO_2$. $MnO_2$ has been considered as a promising alternative class of materials for supercapacitor application due to its low lost and high theoretical capacitance range from 1100 to 1300 F $g^{-1}$.[90] Especially, the chemical and associated electrode potentials of $MnO_2$ in neutral aqueous electrolyte solution ($Na_2SO_4$, $K_2SO_4$ or NaCl solution with pH around 7) are a continuous function of the degree of charge, which is like that of hydrous $RuO_2$. Therefore, as shown in Toupin *et al.*'s report,[91] the CV curve of $MnO_2$ in neutral aqueous electrolyte solution generally exhibits a typical rectangular shape within the potential window from 0–0.9 V (*vs.* Ag/AgCl reference electrode). The charge storage mechanism in the $MnO_2$ electrode, used in aqueous electrolyte,

was investigated by cyclic voltammetry and X-ray photoelectron spectroscopy in Toupin *et al.*'s report. Their result successfully demonstrated that the charge storage of $MnO_2$ was accompanied by the surface state varying from III to IV. Furthermore, the cyclic voltammetry data established that only a thin layer of $MnO_2$ is involved in the redox process and is electrochemically active. Therefore, the specific capacitance of $MnO_2$ is generally much lower than that of $RuO_2$. In other words, the capacitance of $MnO_2$ mainly arises from the surface redox reaction, without capacitance from bulk intercalation. It should be noted that $MnO_2$ is also a typical battery-type electrode for a primary Zn–$MnO_2$ battery in alkaline electrolyte (*e.g.* KOH), or a primary Li–$MnO_2$ battery in an $Li^+$-containing nonaqueous electrolyte, in which the electrode reaction typically involves proton or $Li^+$ intercalation in the crystal lattice. The potential window in an alkaline or nonaqueous electrolyte is different from the potential window for their pseudocapacitive behaviour in neutral aqueous electrolyte. As shown in Fig. 7, the fast and reversible successive surface redox reactions for $MnO_2$ define the behaviour of the voltammogram, whose rectangular shape is close to that of an EDLC. In order to increase the capacitance with an enhanced outside surface area, many types of $MnO_2$ nanostructures with different morphologies have been intensively investigated for supercapacitors, such as nanowires,[92] nanotubes,[93] and flower-like microspheres.[94] For example, our group developed three types of porous $MnO_2$ (ordered mesoporous β-$MnO_2$, disordered mesoporous γ-$MnO_2$, and disordered porous α-$MnO_2$) using hard template, self-assembly, and co-precipitation methods, respectively.[95] The capacitance profiles of the three types of 1D tunnel-structured $MnO_2$ are clearly dependent upon their pore structure, despite their crystalline structure. The three porous $MnO_2$ structures deliver a capacitance of 70–90 μF $cm^{-2}$. Ordered mesoporous β-$MnO_2$ shows a better rate capability due to its ordered mesoporous network, which is more favourable for fast ionic transport. Cheng *et al.* prepared a $MnO_2$ nanowire/graphene composite by solution-phase assembly of graphene sheet and α-$MnO_2$ nanowires.[96] The asymmetric electrochemical capacitor, based on graphene as negative electrode and $MnO_2$ nanowires/graphene composite as positive electrode in a neutral aqueous $Na_2SO_4$ solution as electrolyte, can be cycled reversibly in the high-voltage region of 0–2.0 V and exhibits a superior energy density of 30.4 W h $kg^{-1}$. Chen and co-workers fabricated a nanostructured $MnO_2$/CNT composite on a sponge for supercapacitor application.[97] This novel sponge supercapacitor can reach a high specific capacitance of 1230 F $g^{-1}$ (based on the mass of $MnO_2$) and shows only 4% degradation after 10 000 cycles at a charge–discharge specific current of 5 A $g^{-1}$. In addition to $MnO_2$, $V_2O_5$ also exhibits typical pseudocapacitive characteristics in neutral aqueous electrolyte solution (NaCl or KCl solution with pH around 7), and thus was investigated as a pseudocapacitive electrode for a long time. Recently, Guo and co-workers reported that $V_2O_5$@C core–shell nanowires achieve a remarkable areal capacitance of 128.5 F $cm^{-2}$ at a scan rate of 10 mV $s^{-1}$, with excellent rate capability.[98] Wu and co-workers synthesized a hierarchical porous $V_2O_5$/graphene hybrid aerogel through the *in situ* growth of $V_2O_5$ nanofibers on graphene sheets

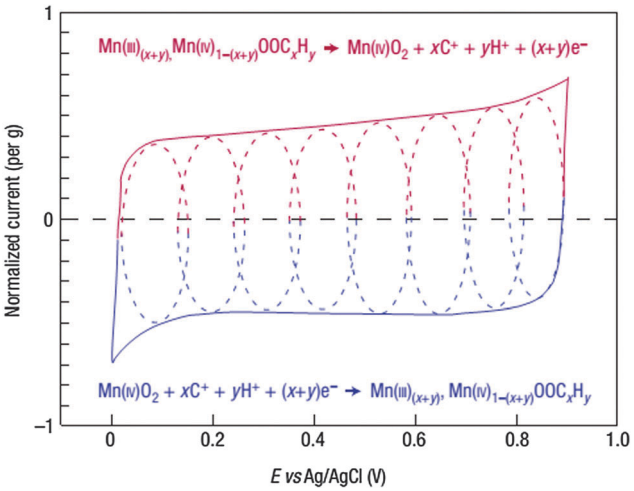


Fig. 7 Cyclic voltammetry. This schematic of cyclic voltammetry for a $MnO_2$-electrode cell in mild aqueous electrolyte (0.1 M $K_2SO_4$) shows the successive multiple surface redox reactions leading to the pseudocapacitive charge storage mechanism. The red (upper) part is related to the oxidation from Mn(III) to Mn(IV) and the blue (lower) part refers to the reduction from Mn(IV) to Mn(III). (Reproduced from ref. 5, with permission from the Nature Publishing Group.)

by a low-cost and facile sol–gel method.[99] The $V_2O_5$/graphene hybrid aerogel-based supercapacitors exhibit enhanced specific capacitance (486 F $g^{-1}$), a high energy density (68 W h $kg^{-1}$), and an outstanding cycle performance.

In recent years, Ni or Co-based oxides and some hydroxides have attracted extensive attention as pseudocapacitive electrode materials.[74,75] Very recently, much effort has been focused on $NiCo_2O_4$ and $NiCo_2S_4$ because of their higher electronic conductivity.[74,100] Owing to previous review articles, we do not list the development of Ni or Co-based materials in detail. As pointed out by Thierry *et al.*, the charge storage of these Ni or Co-based electrodes generally occurs within a very narrow potential range, which is close to that of the typical battery-type electrode of $Ni(OH)_2$, but is different from that of $RuO_2$ or $MnO_2$, which exhibit a potential independent charge storage. Herein, we agree with Thierry *et al.*'s comment that the concept of "capacitance" (F) cannot be applied to the faradaic behaviour of the above electrode materials. In fact, these Ni or Co-based oxides or hydroxide electrodes can only be used to be coupled with carbon-based electrodes to form hybrid supercapacitors, which is similar to $Ni(OH)_2$/carbon hybrid supercapacitors. Therefore, when converted into the unit of capacity (mA h $g^{-1}$), the super-high capacitance value achieved ($>1000$ F $g^{-1}$) cannot facilitate high utilization of electrode materials. However, very little research has been carried out to study their kinetics. Currently, it is too early to conclude that the kinetics of these materials are the same as $Ni(OH)_2$, whose charge is totally controlled by ion diffusion within the crystalline framework.

Generally, it is easy to confuse the concepts of "pseudocapacitive behaviour" and "intercalation pseudocapacitive behaviour". To clarify their difference, the development of the explanation of pseudocapacitive behaviour is schematically illustrated in Fig. 8. In 1991, Conway described the electrochemical

 

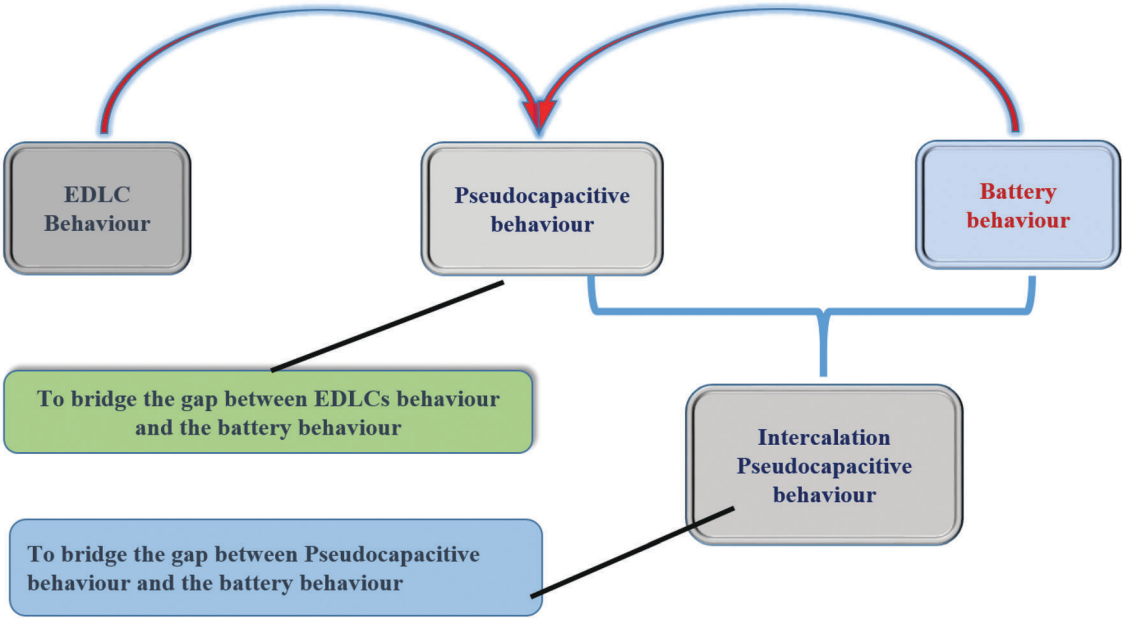


Fig. 8 Schematic of the relationship between different energy-storage mechanisms.

behaviour of $RuO_2$ as a "Transition from "supercapacitor (*i.e.* EDLCs)" to "battery" Behaviour in Electrochemical Energy Storage".[7] In other words, the electrochemical behaviour of $RuO_2$ bridges the gap between the electrochemical behaviour of EDLCs and battery behaviour (Fig. 8). Because the electrochemical profile (*e.g.* the rectangular shape of CV curve) and the fast kinetics (*b*-value in eqn (2) is equal to 1) of the electrodes are all close to that of EDLCs, the electrode behaviour of $RuO_2$ was considered as pseudocapacitive behaviour. In fact, the "intercalation pseudocapacitive behaviour" displays kinetics that are similar to typical pseudocapacitive behavior (*i.e.* a linearly proportional voltammetric response), whereas its electrochemistry is the same as that of battery-type electrode behaviour (*i.e.* redox reaction accompanied by the intercalation of cations in the crystalline framework of electrode materials) (Fig. 8). In other words, its electrochemical profile (*e.g.* clear redox peaks in CV curves) is similar to that of battery behaviour, while its kinetics (*b*-value = 1) and reversibility are higher than those of battery behaviour and are close to those of the conventional pseudocapacitive behaviour of $RuO_2$ or $MnO_2$.

### 3.3 Metal Oxides with intercalation pseudocapacitive behaviour

In 2005, Kavan *et al.*[17] reported pseudocapacitive $Li^+$ intercalation/de-intercalation in $TiO_2$(B), which is conventionally considered as a promising anode material for Li-ion batteries.[10,101] They prepared phase-pure $TiO_2$(B) with microfibrous morphology from amorphous $TiO_2$, and then demonstrated that Li-insertion into the crystalline framework of $TiO_2$(B) is governed by a pseudocapacitive faradaic process. In their CV investigation, the redox peak current ($i_p$) of as-prepared $TiO_2$(B) varied linearly with the sweep rates [$b$ = 1; see eqn (1)], indicating typical pseudocapacitive $Li^+$ intercalation/de-intercalation. Kavan *et al.* discussed this unusual behaviour in terms of the crystal structure of $TiO_2$(B), and assumed that the novel pseudocapacitive intercalation could be ascribed to many freely accessible parallel channels for $Li^+$ transport, perpendicular to the (010) face. Then, Li *et al.*[18] also demonstrated the pseudocapacitive characteristics of $Li^+$ intercalation/de-intercalation in hydrogen titanate nanotubes by detailed CV methods, and claimed that the pseudocapacitive behaviours could be ascribed to the open layered scrolling cross-section with a much larger inter-layer spacing than normal Li intercalation materials. Recently, our group prepared layered $H_2Ti_6O_{13}$-nanowires, and investigated their Li-storage behaviour in a non-aqueous electrolyte.[20] The achieved results also demonstrated the pseudocapacitive characteristics of Li-storage in the layered $H_2Ti_6O_{13}$-nanowires, which is because of the typical nanosize and expanded interlayer space. In our CV investigation, the redox peak current ($i_p$) of as-prepared $H_2Ti_6O_{13}$-nanowires varied linearly with the sweep rates [$b$ = 1; see eqn (1)], which is similar to previous reports.[17–19] Besides the intercalation pseudocapacitance from these titanium oxides, Dunn *et al.* recently reported that orthorhombic $Nb_2O_5$ (T-$Nb_2O_5$) also displays intercalation pseudocapacitive behaviour.[21] Very recently, they further investigated the Li-ion intercalation pseudocapacitance of T-$Nb_2O_5$, and quantified the kinetics of charge storage in T-$Nb_2O_5$ (Fig. 9a and b).[23]

On the other hand, it was also found that for some electrode materials, only part of the capacity arises from intercalation pseudocapacitance, but the intercalation pseudocapacitance contributes to a large portion of the overall capacity. For these materials, the relationship between the redox peak current ($i_p$) and sweep rate ($v$) can also be summarized by eqn (1) (*i.e.* $i_p = av^b$), but the *b*-value is only close to and slightly less than 1, which is different from the investigations mentioned above. In other words, these materials exhibit a hybrid charge storage mechanism, and their current response ($i$) at a fixed potential

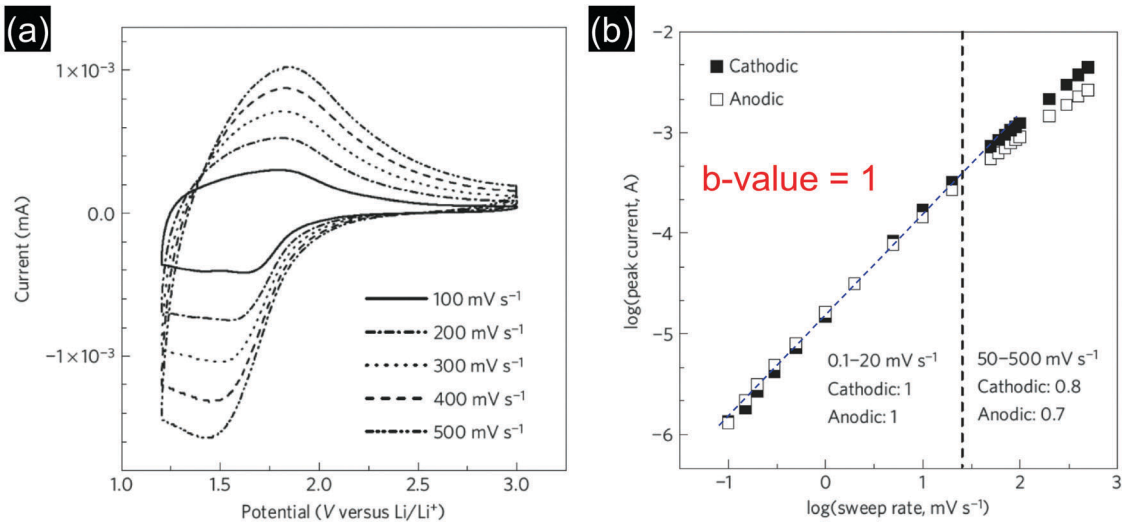


Fig. 9 Electrochemical behaviour of T-$Nb_2O_5$. (a) Cyclic voltammograms from 100 to 500 mV $s^{-1}$. (b) *b*-value determination of the peak anodic and cathodic currents (*i.e.* $i_p$ *vs.* *v*) shows that this value varies from approximately 1 up to 50 mV $s^{-1}$. (Reproduced from ref. 23, with permission from the Nature Publishing Group.)

(*V*) can be described as a combination of two separate mechanisms, namely capacitive effects ($k_1v$) and diffusion-controlled insertion ($k_2v^{1/2}$) according to (4).[22]

Based on eqn (4), Brezesinski *et al.* found that for mesoporous iso-oriented α-$MoO_3$, the capacitive contribution is 70% of the total charge storage (Fig. 10a).[22] Furthermore, Brezesinski *et al.* employed eqn (1) as a function (*i.e.* $i = av^b$) to calculate the current response (*i*) of mesoporous iso-oriented α-$MoO_3$ at different potentials (*V*), and confirmed that the *b*-value varies from 0.8 to 1.0 in the potential window, 1.5–2.6 V *vs.* $Li/Li^+$ (Fig. 10b). With a similar method, Sathiya *et al.* investigated the electrochemical behaviour of a $V_2O_5$/CNT composite for Li-storage, and demonstrated that the capacitive behaviour dominates the intercalation as 2/3 of the overall capacity value out of 2700 C $g^{-1}$ is capacitive, while the remainder is due to diffusion-controlled Li-ion intercalation.[24]

As reviewed above, a "*b*-value" that is equal/or close to 1 should be the key characteristic of intercalation pseudocapacitance in electrode materials. However, some super-fast charge/discharge performances from nanosized battery electrode materials were still misconsidered as pseudocapacitive intercalation. For example, Yang *et al.* very recently reported amorphous $Ni(OH)_2$ nanospheres as a high performance pseudocapacitive electrode material, indicating that $H^+$ intercalation/de-intercalation is a pseudocapacitive characteristic.[102] However, in their CV investigation, it can be clearly seen that the relationship between the peak current ($i_p$) of as-prepared $Ni(OH)_2$ and the sweep rate (*v*) should almost be presented by $i_p = av^{0.5}$ (*i.e.* *b*-value is 0.5), indicating typical diffusion-controlled charge storage (Fig. 11a and b). In other words, the reported $Ni(OH)_2$ is still a battery electrode material, rather than a pseudocapacitor material. A *b*-value that is equal or close to 0.5 also indicates that the

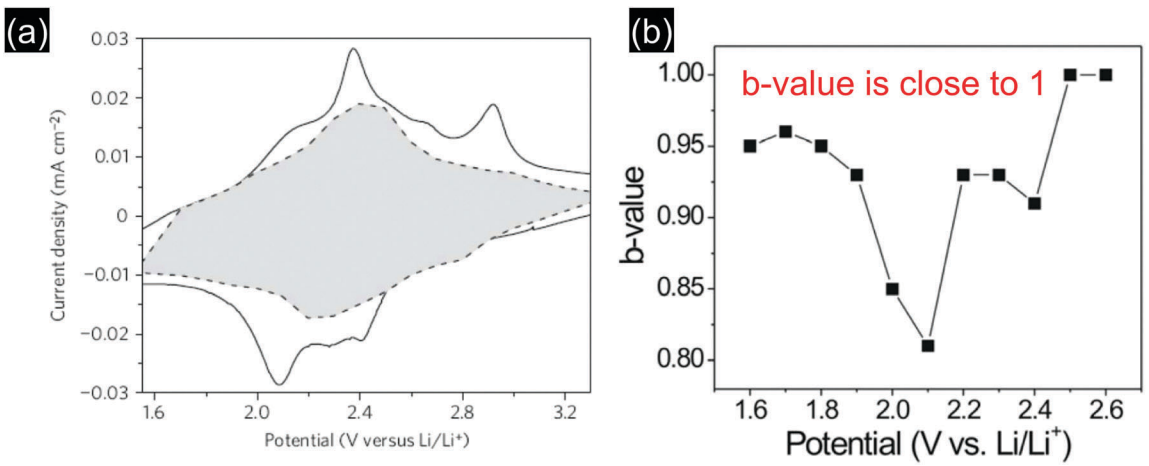


Fig. 10 Electrochemical behaviour of ordered mesoporous a-$MoO_3$. (a) Voltammetric responses for mesoporous $MoO_3$ films at a sweep rate of 0.1 mV $s^{-1}$, where the capacitive contribution (~70%) to the total current is shown by the shaded region. (b) Power-law dependence of charge storage kinetics for mesoporous a-$MoO_3$ as a function of potential (cathodic sweep). (Reproduced from ref. 22, with permission from the Nature Publishing Group.)

 

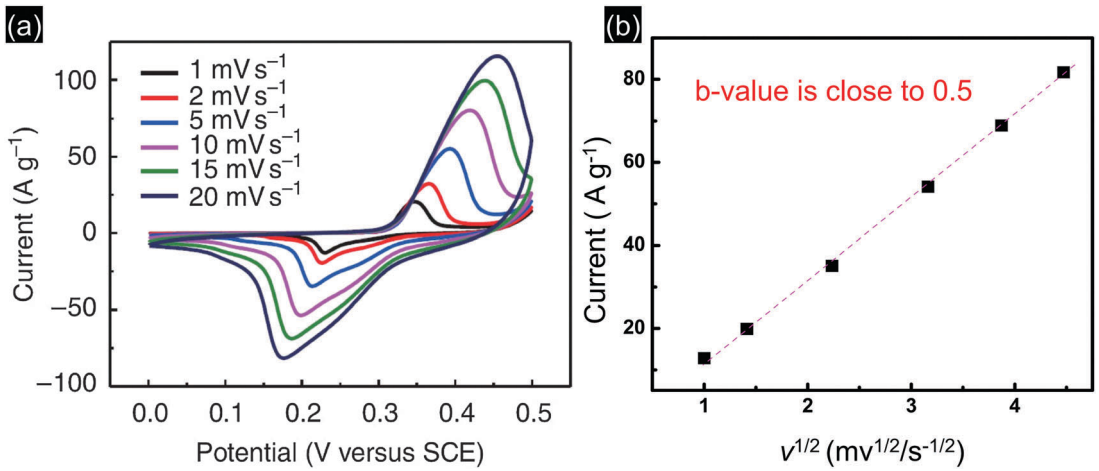


Fig. 11 Electrochemical behaviour of amorphous nickel hydroxide. (a) CV curves at various scan rates in 1 M KOH. (b) *b*-Value determination of cathodic currents ($i_p$ *vs.* $v^{0.5}$) shows that this value is approximately 0.5 up to 20 mV $s^{-1}$. (Reproduced from ref. 102, with permission from the Nature Publishing Group; (b) is evaluated from peak current on negative sweep in (a)).

pseudocapacitance contribution is very small or negligible. It can be assumed that the surprising charge/discharge performance presented in Yang *et al.*'s report should be ascribed to the super-low mass loading (0.1 μg),[102] which is rarely employed for battery investigation. It is well known that the true performance of an electrode is dependent on the mass-loading active materials, and this been well discussed by Gogotsi *et al.*, recently.[103] As regards the intercalation pseudocapacitance mechanism, a high capacitance can still be retained, even at high mass loading of electrode materials. For instance, in Dunn *et al.*'s recent report, a 40 μm thick T-$Nb_2O_5$ (1 mg $cm^{-2}$) electrode still exhibits very fast charge/discharge characteristics.[23] The peak current ($i_p$) of the thick T-$Nb_2O_5$ electrode linearly increased with the sweep rate ($v$), indicating a *b*-value that is equal to 1. Accordingly, the rate capability for T-$Nb_2O_5$ is significantly better than the high-rate $Li_4Ti_5O_{12}$ above 30 C and, even at a 1000 C rate, the capacity of the thick T-$Nb_2O_5$ electrode is ~40 mA h $g^{-1}$. By the way, nanosized $Ni(OH)_2$ has been "misreported" as a pseudocapacitor material for a long time,[104–109] owing to its application in a hybrid supercapacitor that is based on a battery electrode $Ni(OH)_2$ and an EDLC electrode (*e.g.* activated carbon).[110,111] Herein, we clarify this point to further emphasize the characteristics of intercalation pseudocapacitance.

It is undoubted that each nanosized battery electrode material should exhibit pseudocapacitive behaviour that is based on the surface redox reactions, because many metal ions within the bulk have been exposed to the outer surface. However, the capacity (or capacitance) contribution from the surface pseudocapacitive behaviour is small or even negligible, compared with the overall capacity of the electrode. For example, the amorphous $Ni(OH)_2$ nanospheres reported by Yang *et al.*[102] should have a high surface area, but the capacitive contribution of the as-prepared $Ni(OH)_2$ is still almost negligible (see Fig. 11). Our recent investigation on graphene-supported $Ni(OH)_2$ nanowires also confirms this point.[111] A similar phenomenon can be detected in the electrochemical performance of nanosized $LiFePO_4$, which is a famous positive electrode material for current Li-ion batteries. Ceder *et al.* have demonstrated that nanosized $LiFePO_4$ can display supercapacitor-like fast charge/discharge with a low mass loading of the electrode.[112] Very recently, we investigated the pseudocapacitive profile of nanosized $LiFePO_4$, confirming its supercapacitor-like fast charge/discharge and demonstrating that the total capacitive contribution is ~10% of the overall capacity through various electrochemical analytical methods.[113] Furthermore, Wang *et al.* demonstrated that the total capacitive contribution of 10 nm anatase $TiO_2$ (surface area 150 $m^2$ $g^{-1}$) is less than 10% of the overall capacity, because the $Li^+$ intercalation in anatase $TiO_2$ is still limited by the diffusion process.[19] Unlike conventional surface pseudocapacitance, charge storage in intercalation pseudocapacitance does not occur on the surface but in the bulk of materials. Therefore, if an electrode displays intercalation pseudocapacitance, its capacitive contribution generally dominates the overall capacity (or capacitance), such as in $TiO_2$(B), $H_xTi_xO_y$, T-$MoO_3$, and T-$Nb_2O_5$.

Although we have reviewed recent progress in intercalation pseudocapacitance, it is still necessary to summarize its characteristics, which may help readers to further understand what intercalation pseudocapacitance is, and how to design an electrode material with intercalation pseudocapacitance. Herein, we summarize the characteristics of intercalation pseudocapacitance as follows:

(1) Electrochemical performance without diffusion control: as mentioned above, the electrochemical features of intercalation pseudocapacitance are a linearly proportional voltammetric response (currents *vs.* sweep rates), peak potentials that do not shift significantly with sweep rate, and a capacitive contribution that dominates the overall capacity. Besides these electrochemical features, electrode materials with intercalation pseudocapacitance generally exhibit slope charge/discharge curves within a wide potential window, which is different from conventional battery electrode materials.

(2) Intercalation with negligible crystallographic phase changes: in many Li-ion (or proton) intercalation materials,

the charge storage is generally accompanied by crystallographic phase change. Especially, peak potentials observed in the CV investigation of such battery electrode materials generally shift significantly, with an increase in sweep rate, indicating a high irreversible energy density between charge and discharge. However, Dunn *et al.* have demonstrated that there are no apparent phase and lattice constant changes in the charge storage of T-$Nb_2O_5$.[23] In our recent work about the intercalation pseudocapacitance of $H_2Ti_6O_{13}$, it can be seen that the XRD pattern of an Li-intercalated $H_2Ti_6O_{13}$ electrode is almost the same as that of a fresh $H_2Ti_6O_{13}$ electrode, indicating a negligible phase change.[20] Therefore, one of the key characteristics of intercalation pseudocapacitance is charge storage without phase transformation.

(3) Two-dimensional (2D) ion diffusion pathways: as reviewed above, electrode materials with intercalation pseudocapacitance (*e.g.* $H_xTi_yO_x$, $V_2O_5$, $MoO_3$, and $Nb_2O_5$) exhibit an open, layered structure that enables fast ion transport within the active materials. Charge storage that behaves as a quasi-2D process exhibits similar behaviour to a 2D adsorption reaction. These characteristics are different from those of pseudocapacitive $RuO_2{\cdot}xH_2O$ or $MnO_2{\cdot}yH_2O$, where charge storage occurs mainly on the surface or near-surface. Therefore, a layered structure should also be important for designing electrode materials with intercalation pseudocapacitance.

### 3.4 Conducting polymers with pseudocapacitive behaviour

It is well known that conducting polymers, including polyacetylene (PA), polypyrrole (PPy), polyaniline (PANI), and poly(3,4-ethylenedioxythiophene) (PEDOT) have been considered as promising pseudo-capacitive electrode materials for supercapacitors due to their prominent properties. Conducting polymers are rendered conductive through a conjugated bond system along the polymer backbone. They offer capacitive behaviour through redox reactions that occur not only on the surface, but also throughout the entire bulk. The redox processes are highly reversible because no structural changes, such as phase transformation, happen during the redox reactions. In the family of conducting polymers, PANI and PPy are the most promising members due to their low cost, environmental stability and facile synthesis. Since the n-doping potentials of PANI and PPy are far below the reduction potential of a common electrolyte, both of them can only be p-doped. Therefore, they are usually applied as positive electrode materials. It is noted that a proton is required during charging and discharging of PANI. Hence, an acidic solution, a protic solvent, or a protic ionic liquid should be considered when choosing the electrolyte.

Many researchers have reported on employing conducting polymers in supercapacitors. For instance, PANI hydrogels, combinations of conducting polymers and hydrogels, have been synthesized *via* oxidative coupling reactions in the absence of any additional crosslinkers by using ammonium persulfate as the oxidizing agent and aniline hydrochloric salt as the precursor.[114] The PANI hydrogel electrodes exhibit a high capacitance of 750 F $g^{-1}$ at a current load of 1 A $g^{-1}$. Huang *et al.* deposited PPy on stretchable stainless steel mesh, which exhibits a capacitance of up to 170 F $g^{-1}$ at a specific current of 0.5 A $g^{-1}$ in a solid-state supercapacitor.[115]

Unfortunately, conducting polymers may swell and shrink in the process of intercalation and de-intercalation, which often results in a low cycling stability when they are used in supercapacitors. The chain structure, electrical conductivity, mechanical stability, processability, and mitigation of mechanical stress of conducting polymers can be improved by compositing with other species, which will improve their cycling stability. For instance, Wang and co-workers synthesized cobalt-based MOF (ZIF-67) onto carbon cloth and further electrically deposited PANI to give a flexible conductive porous electrode without altering the underlying structure of the MOF.[116] This type of composite exhibits an extraordinary areal capacitance of 2146 mF $cm^{-2}$ at 10 mV $s^{-1}$, higher than that of a PANI/carbon cloth electrode (727 mF $cm^{-2}$). Zhao and co-workers developed a polyaniline-coated hierarchical porous carbon composite *via* a vapor deposition polymerization approach. This composite structure delivers a high capacitance of 531 F $g^{-1}$ at a current load of 0.5 A $g^{-1}$, and an outstanding cycling stability with capacitance retention of 96.1% after 10 000 cycles.[117] Liu and co-workers constructed a type of three-dimensional highly ordered graphene–PANI hybrid material that displays a high specific capacitance (1225 F $g^{-1}$), an outstanding rate capability, and an excellent cycling stability, which is ascribed to amplified synergistic effects resulting from better exfoliation and stability of graphene sheets, highly ordered PANI nanorods and interface conjugation.[118] Wang *et al.* prepared a nanocellulose-coupled PPy@graphene oxide paper *via in situ* polymerization for use in supercapacitors, exhibiting stable cycling over 16 000 cycles at 5 A $g^{-1}$ and a large specific volumetric capacitance of 198 F $cm^{-3}$.[119] Additionally, the cycling stability of conducting polymers can be improved in a suitably selected potential window.[120] And the ideal capacitive behaviour can be achieved when keeping conducting polymers in the conducting state.

### 3.5 Electrolyte for supercapacitor

The electrolyte, including solvent and salt, is one of the most important constituents of electrochemical supercapacitors due to its advantages of ionic conductivity and charge compensation on both electrodes of the cell. Up to now, various types of electrolytes have been developed by researchers. These electrolytes can be classified as organic electrolytes, aqueous electrolytes, ionic liquids, and solid-state polymer electrolytes. And the main electrolytes currently used for supercapacitors are listed in Table 1.

Conducting salts dissolved in organic solvents constitute the organic electrolytes of supercapacitors; these can provide a voltage window of 3.5 V, which is much wider than that of aqueous electrolytes. However, there are still some drawbacks associated with organic electrolytes, such as higher cost, lower specific capacitance, and inferior conductivity, as well as safety concerns associated with flammability, volatility, and toxicity. The typical organic electrolytes for commercial electrochemical double-layer capacitors (EDLC) consist of conductive salts (*e.g.*, tetraethylammonium tetrafluoroborate ($TEABF_4$)) dissolved in acetonitrile or propylene carbonate (PC) solvent. Although acetonitrile can

 

Table 1 The main electrolytes currently used for supercapacitors

| Electrolyte | Voltage window (V) | Ref. |
|---|---|---|
| TEABF4/PC | 3.5 | 119 |
| $H_2SO_4$ | 1.0 | 120 |
| KOH | 1.0 | 120 |
| $Na_2SO_4$ | 1.8 | 120 |
| $Li_2SO_4$ | 2.2 | 120 |
| Pyrrolidinium dicyanamide | 2.6 | 121 |
| PVA/$H_3PO_4$ hydrogel | 0.8 | 124 |

dissolve much more salt than other solvents, it is harmful to the environment. In contrast, PC-based electrolytes are not only friendly to the environment, but also provide a wide voltage window, a wide range of working temperatures, and good electrical conductivity. Therefore, the organic electrolyte, $TEABF_4$/PC, has been widely used in EDLC studies.[121] However, two issues should be kept in mind. One is that the ion size of the selected electrolyte should be matched with the pore diameter of carbon materials to achieve the maximum specific capacitance. Otherwise, the accessibility for electrolyte ions will be limited. The other is that organic electrolytes must contain very little water, that is, below 3–5 ppm. Otherwise, the capacitor's voltage will be greatly reduced.

By contrast, aqueous electrolytes can offer a higher ionic concentration, a lower resistance and a much higher ionic conductivity than organic electrolytes. For instance, the ionic conductivity for 1 M $H_2SO_4$ and 6 M KOH at 25 °C is about 0.8 and 0.6 S $cm^{-1}$, respectively.[122] Generally, aqueous electrolytes can be divided into acid, neutral and alkaline solutions, among which $H_2SO_4$, KOH, and $Na_2SO_4$ are the most popular and representative electrolytes. Even so, aqueous electrolytes still show a significant disadvantage in a much lower potential window (about 1.2 V) than organic electrolytes, which is restricted by water decomposition. These three types of electrolytes can be applied in carbon-based EDLCs, pseudo-capacitors, and hybrid supercapacitors. It is noted that the essence of the electrolyte significantly affects the pseudo-capacitive properties of carbon-based electrode materials due to the different behaviour of surface functionalities in different electrolytes. For instance, pyridinic-type nitrogen, pyrrolic-type nitrogen, and quinone-type oxygen on the surface of carbon materials could produce pseudo-capacitive effects in $H_2SO_4$ aqueous electrolyte, associated with the proton-involved redox processes, as shown in eqn (5):[64]

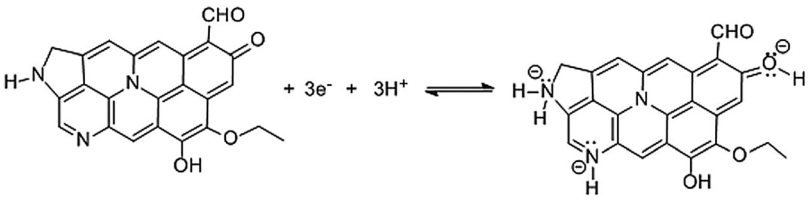


(5)

However, this effect was hardly observed in alkaline and neutral electrolytes. Therefore, it seems to be quite important to generate profitable surface functionalities on the carbon-based electrode materials by selecting suitable electrolytes, in order to achieve an optimum supercapacitor performance.

Recently, ionic liquids have received significant interest as alternative electrolytes for supercapacitors because of their negligible volatility, high thermal, chemical and electrochemical stability, low flammability, and wide electrochemical stability window of 4.5 V, as well as good conductivity of *ca.* 10 mS $cm^{-1}$.[122] Ionic liquids, usually composed of a large asymmetric organic cation coupled with an inorganic or organic anion, behave like molten salts or fused salts at room or lower temperatures and require no voltage-limiting solvents in charge transportation. Benefitting from the conjugation of particular cations and anions, ionic liquids have a low melting point below 100 °C. The main ionic liquids investigated for supercapacitors are pyrrolidinium, imidazolium or aliphatic quaternary ammonium salts coupled with such anions as $PF_6^-$, $BF_4^-$, $TFSI^-$, or $FSI^-$. It is a challenge to design or select suitable ionic liquid electrolytes for EDLCs, which should possess a high ionic conductivity, a broad potential window and a wide range of working temperatures. It was reported that fluorine-free and solvent-free pyrrolidinium dicyanamide ionic liquids are excellent candidates to be employed as electrolytes in EDLCs, which was ascribed to their high ionic conductivity.[123] And the ionic conductivity of the ionic liquid electrolyte could be further improved by adding a small amount of single-walled CNTs (0.1 or 0.5 wt%), resulting in enhanced capacitance, energy density and cycling stability.[124]

Solid polymer electrolyte-based supercapacitors have attracted great interest in recent years due to the rapidly growing demand for power for various types of electronics. The solid polymer electrolytes can act as ionic conducting media and electrode separators. There are three types of polymer-based solid electrolyte for supercapacitors: dry polymer electrolyte, gel polymer electrolyte, and polyelectrolyte. Among these, the gel polymer electrolyte has recently been the most extensively investigated electrolyte because of its high ionic conductivity. Additionally, the gel polymer electrolyte is known as a hydrogel polymer electrolyte when using water as the plasticizer. And this type of hydrogel polymer electrolyte generally possesses three-dimensional polymeric networks. Owing to easy preparation, good hydrophilicity, outstanding film-forming properties, non-toxic features, and low cost, poly(vinyl alcohol) (PVA) has been the most greatly investigated polymer matrix to date, and is commonly mixed with other aqueous solutions.[125] For example, Chen and co-workers[126] synthesized six different types of PVA-based hydrogel electrolytes by employing different aqueous solutions, such as $H_3PO_4$, $H_2SO_4$, KOH, NaOH, KCl, and NaCl, among which the PVA/$H_3PO_4$ electrolyte delivered the best capacitive performance. Additionally, as a famous proton-conducting polymer, the perfluorosulfonic acid polymer known as Nafion has also been applied as the

electrolyte in solid supercapacitors owing to its high ionic conductivity.[127,128]

Recently, redox couples have been added into the electrolyte to promote rapid faradaic reactions for carbon electrodes. For instance, Zhang's group[129] reported a capacitance enhancement of Co–Al layered double hydroxide *via* adding hexacyanoferrate(II) and (III) solely or jointly into 1 M KOH electrolyte, in which the $Fe(CN)_6^{3-}/Fe(CN)_6^{4-}$ ion pair serves as an electron relay at the electrode/electrolyte interface in the process of charge/discharge by coupling the redox reaction of Co(II)/Co(III) in the Co–Al layered double hydroxide electrode. Additionally, Mai and co-workers[130] reported a new type of $CuCl_2$–$HNO_3$ redox-active electrolyte. Through utilizing $Cu^{2+}$ reduction and carbon–oxygen surface groups of the electrode, the voltammetric capacitance (4700 F $g^{-1}$) is greatly improved by 10 fold compared to a conventional electrolyte.

# 4. Supercapacitor systems

According to the composition difference of electrode materials, supercapacitor devices can be classed as follows: symmetric supercapacitor, asymmetric supercapacitor, and hybrid supercapacitor. However, there is still confusion associated with distinguishing an asymmetric supercapacitor from a hybrid supercapacitor. Herein, we will briefly summarize the characteristics of symmetric, asymmetric, and hybrid supercapacitors, as well as the latest advances in these.

## 4.1 Symmetric supercapacitors

Symmetric supercapacitors are typically composed of two identical supercapacitor-type electrodes, including AC and pseudo-capacitive materials. Most commercial supercapacitors are based on two symmetric AC electrodes in organic electrolytes, whose voltage window can reach 2.7 V.[131] As mentioned above, the limited operating voltage of aqueous electrolytes is about 1.23 V, being restricted by water decomposition. Therefore, the key point in further increasing the energy density of an aqueous electrolyte-based supercapacitor is widening the voltage window. Recently, an excellent cycle life under galvanostatic charge/discharge up to 1.6 V has been demonstrated for AC//AC symmetric capacitors in 0.5 M $Na_2SO_4$ aqueous electrolyte.[132] Later, Beguin's group reported that the voltage of an AC//AC symmetric capacitor can reach 1.9 V in 2 M $Li_2SO_4$ aqueous electrolyte.[133] The AC//AC symmetric supercapacitor reported by Hu *et al.* exhibits a high cell voltage of 2.0 V in 0.5 M $Na_2SO_4$ aqueous electrolyte.[134] Such a high value is attributed to the high over-potential related to the hydrogen storage mechanism. Moreover, Xia and co-workers built a symmetric aqueous supercapacitor using $RuO_2$ as both negative and positive electrode, achieving a high operating voltage of 1.6 V with high energy density and power density.[135] Such a good performance is due to the high over-potential of $RuO_2$ for oxygen evolution. Therefore, one useful strategy for widening the voltage window is to select electrode materials that have high over-potentials for hydrogen and/or oxygen evolution. Recently, symmetric supercapacitors based on porous activated carbon[136] and reduced graphite oxide,[137] with voltage windows of 1.8 and 1.6 V, respectively, have also been reported. It is noted that, although the symmetric supercapacitors are using the same supercapacitor-type materials as the positive and negative electrode, the masses of the two electrodes are different based on the different electrolyte ions absorbed on the positive and negative electrodes during the charge–discharge process.

## 4.2 Asymmetric supercapacitors

Asymmetric supercapacitors are composed of two different supercapacitor-type electrodes, one electrode being of a double-layer carbon material and the other being of a pseudocapacitance material. AC//$MnO_2$ is one type of promising asymmetric supercapacitor and has recently been widely studied for energy storage. For example, Brousse and co-workers reported that the asymmetric supercapacitor, AC//$MnO_2$, tested in a mild aqueous electrolyte (0.65 M $K_2SO_4$), can be reversibly cycled between 0 and 1.5 V with negligible gas evolution.[138] A real energy density of 10 W h $kg^{-1}$ was reproducibly measured, with a real power density reaching 3600 W $kg^{-1}$. Qu and co-workers reported that an asymmetric AC/$K_2SO_4$/$MnO_2$ supercapacitor could be cycled reversibly between 0 and 1.8 V, with an energy density of 17 W h $kg^{-1}$ at a power density of 2 kW $kg^{-1}$.[139] Long and co-workers assembled an AC//$MnO_2$ asymmetric supercapacitor with a 5 M $LiNO_3$ solution as electrolyte, which circumvented the main limitation of aqueous electrolytes by extending their operating voltage window beyond the thermodynamic 1.2 V limit to operating voltages approaching ~2 V, resulting in high power and energy density.[140] Hu and co-workers employed sodium-doped $MnO_2$ as positive electrode and AC as negative electrode to assemble an asymmetric supercapacitor, whose cell voltage can reach 2.4 V.[141] Additionally, asymmetric supercapacitors based on $V_2O_5$/electrospun carbon fiber composite and electrospun carbon fiber,[142] hierarchical $NiMoO_4$ and AC,[143] graphene foam (GF)/carbon nanotubes, (CNT)/$MnO_2$, and GF/CNT/PPy[144] have also been extensively studied recently and demonstrate outstanding electrochemical performances. Besides, Rajkumar *et al.* have recently reviewed the advances in aqueous asymmetric and hybrid supercapacitors.[145]

## 4.3 Hybrid supercapacitors

Hybrid supercapacitors are typically composed of a supercapacitor-type electrode and a battery-type electrode.[146–150] Recently, many hybrid systems have been reported in aqueous or nonaqueous electrolytes, such as AC//$PbO_2$, AC//$Ni(OH)_2$, AC//$Li_4Ti_5O_{12}$, AC//graphite, and AC//$LiMn_2O_4$. According to Thierry *et al.*'s report,[26] Ni-based or Co-based electrodes should be described as pseudocapacitive electrodes, rather than battery-type electrodes. Therefore, AC//$Co_3O_4$[151] and AC//NiO[152] cells are classified as hybrid supercapacitors, and these have also been widely investigated recently. In this section, the progress of some hybrid supercapacitors is briefly summarized.

**4.3.1 AC//$PbO_2$.** Among the different hybrid supercapacitors available, AC//$PbO_2$ seems to be one of the best choices due to its high voltage (about 2 V in aqueous electrolyte) and the low cost of AC, $PbO_2$, and sulfuric acid. An AC//$PbO_2$ hybrid system in 5.3 M $H_2SO_4$ has been designed by Yu and Gao.[153] The hybrid

 

supercapacitor can deliver a specific capacitance of 71.5 F $g^{-1}$ at a discharge current density of 200 mA $g^{-1}$ and a specific energy of 32.2 W h $kg^{-1}$ in the potential range 0.8–1.8 V. Despite the many advantages of this aqueous-based hybrid device, the limited cyclability and power capability of the $PbO_2$ positive electrode will limit the electrochemical performance of the hybrid cell. In order to overcome these two limitations of the positive electrode, Perret *et al.* proposed to couple the two approaches of electrolyte change and $PbO_2$ nanostructuration.[154] They applied an AC negative electrode, $PbO_2$ thin film, and a nanowire array positive electrode with an electrolyte made of a lead salt dissolved in methane sulfonic acid to assemble a new hybrid supercapacitor. This type of hybrid system exhibits a specific capacitance of 34 F $g^{-1}$ and a specific energy density of 29 W h $kg^{-1}$, and does not show any sign of degradation during more than 5000 cycles.

**4.3.2 AC//$Ni(OH)_2$.** For a hybrid supercapacitor based on $Ni(OH)_2$ and AC, using KOH solution as electrolyte, the positive electrode material, $Ni(OH)_2$, converts to NiOOH during the charge process according to the following reaction:

$$Ni(OH)_2 \rightarrow NiOOH + H^+ + e^- \quad (6)$$

The discharge process is the reverse of eqn (6). Accordingly, the energy density of the capacitor is critically dependent on the energy density of the AC electrode material and the cell working voltage, but the power density depends on the rate capability of the battery electrode. Obviously, the rate capability of $Ni(OH)_2$ is associated with proton diffusion in the $Ni(OH)_2$ framework. In order to obtain a high rate capability, it is necessary to develop a nanosized $Ni(OH)_2$ material. Park *et al.* fabricated a hybrid supercapacitor with a $Ni(OH)_2$/AC composite as a positive electrode and an AC as a negative electrode.[155] For the hybrid capacitor, a maximum specific capacitance of 540 F $g^{-1}$ and a specific energy density of 25 W h $kg^{-1}$ were obtained. Our group designed a hybrid supercapacitor based on an AC negative electrode and a $Ni(OH)_2$/CNT composite (the well-distributed, nanosized $Ni(OH)_2$ was loaded on the surface of CNTs) positive electrode.[108] The composite provides a shorter diffusion path for proton diffusion and larger reaction surface areas, as well as reducing the electrode resistance due to the high electronic conductivity of the carbon nanotubes. As a result, the rate capability and utilization of $Ni(OH)_2$ was greatly improved. The hybrid cell delivered a specific energy of 32 W h $kg^{-1}$ at a specific power of 1500 W $kg^{-1}$, based on the total weight of the active electrode materials. It also exhibited a good cycling performance and kept 90% of its initial capacity for over 2000 cycles.

**4.3.3 AC//$Li_4Ti_5O_{12}$.** The Li-ion-intercalated compound, $Li_4Ti_5O_{12}$, has an excellent Li-ion insertion/extraction reversibility and exhibits no structural changes (zero-strain insertion material) during charge–discharge cycling. Recently, spinel $Li_4Ti_5O_{12}$ has been demonstrated as the most promising electrode material for hybrid supercapacitors. For example, Amatucci *et al.*[156] used a positive electrode material of AC and a negative electrode material of nanostructured $Li_4Ti_5O_{12}$ to assemble a hybrid cell, which exhibits a sloping voltage profile from 3 to 1.5 V, 90% capacity utilization at 10 C charge/discharge rates, and a 10–15% capacity loss after 5000 cycles. Pasquier *et al.*[157] built a 500 F hybrid supercapacitor using a nanostructured $Li_4Ti_5O_{12}$ negative and an AC positive electrode. The 500 F device has a usable packaged specific energy of 11 W h $kg^{-1}$, with a specific power of 800 W $kg^{-1}$ at 95% efficiency. Our group applied nanosized $Li_4Ti_5O_{12}$, synthesized by a molten salt process, as the negative electrode material of a $Li_4Ti_5O_{12}$//AC hybrid supercapacitor, which shows much better rate capability.[158] Even at a 100 C discharge rate, the hybrid cell retains 60% of capacity compared with a 3 C discharge rate. However, the $Li_4Ti_5O_{12}$//AC hybrid supercapacitor generally operated at voltages of less than 2.8 V, which results in low utilization of the positive electrode. If operated with a higher voltage of 3 V, gas generation would occur on the electrode. Therefore, Yang *et al.*[159] investigated the possibility of achieving stable operation at 3 V with a $Li_4Ti_5O_{12}$// AC hybrid supercapacitor by balancing the capacitances of the two electrodes on the basis of their voltage profiles at different operating voltages.

**4.3.4 AC//graphite.** Recently, Beguin *et al.*[160] developed a hybrid supercapacitor in an organic electrolyte using graphite and AC as negative and positive electrode materials, respectively (Fig. 12). In the optimized hybrid capacitor, the potential of the positive electrode ranges from 1.5 to 5 V *vs.* $Li/Li^+$, being extended to the whole stability window of AC in the organic electrolyte, whereas the potential of the negative electrode remains almost constant at around 0.1 V *vs.* $Li/Li^+$. As a result, the hybrid cell obtained a high gravimetric density of 103.8 W h $kg^{-1}$ and a high volumetric energy density of 111.8 W h $L^{-1}$. Li and Wang[161] presented a micro hybrid supercapacitor integrating an AC positive electrode and a graphite negative electrode in 1 M $LiPF_6$ electrolyte, using micro electro mechanical systems (MEMS) fabrication technology. The hybrid supercapacitor prototype with 100 μm thick interdigital electrodes has a capacity of 180 μA h $cm^{-2}$ and an energy density of about 1750 mJ $cm^{-2}$ at a charge/discharge current density of 0.5 mA $cm^{-2}$. Especially, graphite is also a suitable positive electrode material for high-energy electrochemical capacitors. Therefore, Wang and Yoshio[162] introduced a novel capacitor with high energy density, in which a graphite electrode was used as the positive electrode, AC only served as the negative electrode, and an organic electrolyte was applied to ensure a high working voltage up to 3.5 V. The potential of the graphite positive electrode can reach a voltage of about 4.78 V *vs.* Li. The mechanism of charge storage at the graphite positive electrode was expected to involve the insertion of anions into interlayer spaces between the graphite layers.

**4.3.5 AC//$LiMn_2O_4$.** $LiMn_2O_4$ has been considered a promising positive electrode material for hybrid supercapacitors due to its very good rate capability. Early in 2005, our group developed a new hybrid supercapacitor using AC as a negative electrode and a lithium-ion-intercalated compound, $LiMn_2O_4$, as a positive electrode in a neutral $Li_2SO_4$ aqueous electrolyte.[163] The Li ions are deintercalated from the framework of the spinel in the charge process and simultaneously adsorbed on the surface of the AC electrode. The reverse process occurs during discharge. This aqueous hybrid system exhibits a sloping voltage profile from 0.8 to 1.8 V and delivers an estimated specific energy of *ca.*

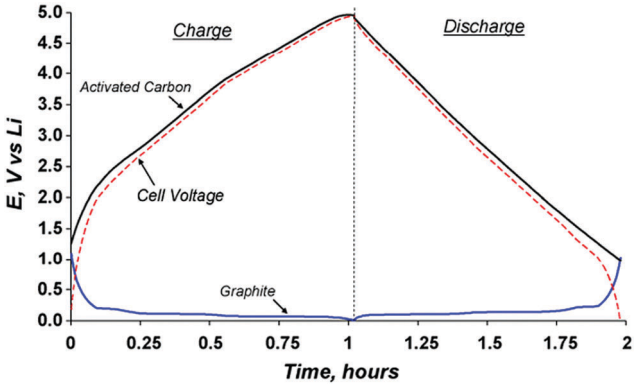


Fig. 12 Galvanostatic charge–discharge at a current density $C$ of the electrodes and cell (dotted line) for a hybrid capacitor utilizing activated carbon as positive electrode and graphite as negative electrode. (Reproduced from ref. 160, with permission from Elsevier.)

35 W h $kg^{-1}$. Subsequently, Cericola and co-workers[164] investigated the rate capability of a hybrid supercapacitor based on a $LiMn_2O_4$ positive electrode and an AC negative electrode. It was found that the contribution of AC is basically unaffected by the discharge rate. The hybrid cell exhibits 'battery like' behaviour at low discharge rates and 'capacitor like' behaviour at high discharge rates. The specific capacitance of the hybrid cell outperforms the AC electrode at low rates and the $LiMn_2O_4$ electrode at high rates. Kwon and co-workers[165] also investigated a similar $LiMn_2O_4$/AC hybrid system using an organic electrolyte, and analyzed the effect of lithium difluoro (oxalate) borate (LiDFOB) as an electrolyte additive on the electrochemical performance of the $LiMn_2O_4$/AC hybrid supercapacitor. It was demonstrated that the LiDFOB additive in the electrolyte can efficiently reduce the charge transfer resistance in the hybrid supercapacitor and retard the phase transition of $LiMn_2O_4$ during repeated charging/discharging cycles.

As mentioned above, many supercapacitor systems have been investigated over the past years. In addition, some of them have been commercialized in recent years (Table 2). The applications of these commercial supercapacitors will be further reviewed in Section 6.

# 5. Characterization methods

## 5.1 Material characterization

Supercapacitors deliver capacitance mainly through the surface reactions of electrode materials. Accordingly, characterization of surface area, pore structure and surface structure (containing functional groups) is necessary. Normally, the surface area and the pore-size distribution, including macro, meso-, and micro-pores can be determined by Brunauer–Emmett–Teller (BET) calculation of the gas adsorption branch in a certain relative pressure range. Non-local density functional theory (NLDFT) analysis of argon adsorption isotherms was typically employed to characterize micro-pores. Also, surface analysis, using FT-IR and XPS, is most important for the pseudo-capacitance electrode materials.

### 5.1.1 Brunauer–Emmett–Teller (BET) method

The surface reaction of electrode materials consists of charge adsorption/desorption at the electrode/electrolyte interface and faradic reactions, which deliver electrochemical double-layer capacitive behaviour and pseudocapacitive behaviour, respectively. As is known to us, the capacitance of supercapacitors is strongly related to the surface area of the selecting electrode materials. However, the electrolyte ions could not access the whole specific surface area. The pore size of the electrode materials markedly affects the electrochemically active surface area. Specific surface area characterization can be performed by nitrogen (77.4 K) or argon (87.3 K) sorption experiments using the Brunauer–Emmett–Teller (BET) method. Additionally, $CO_2$ adsorption/desorption is performed to assess the specific surface area of the ultramicropores with pore diameters less than 1 nm. For instance, Ruoff *et al.*[58] analyzed the pore size distribution from the $CO_2$ and nitrogen adsorption branches of the isotherms by employing a NLDFT and assuming that the pores are slit/cylinder shaped. In their investigation, the adsorption/desorption isotherms under $N_2$, Ar, and $CO_2$ atmospheres were shown as examples (Fig. 13A).[58] Normally, the pore size distribution, including mesopores and micropores, can be determined from $N_2$ or Ar adsorption isotherms, using a non-local density functional theory (NLDFT). Micro-pore-based charge storage can efficiently improve the electrochemical double-layer capacitance, and thus has attracted extensive attention in recent years. Especially, a $CO_2$ atmosphere can more accurately detect ultramicropores less than 1 nm. A pore geometry with slits, cylinders, or both should be chosen when using the NLDFT, according to the material nature. As shown in Fig. 13B, the analysis of $CO_2$ data reveals the presence of ultramicropores, while the pore size distribution curve for $N_2$ adsorption confirms the presence of micropores centered at above 1 nm in size, and narrow mesopores with a diameter of 4 nm.

Table 2 Technology approaches for the development of commercial supercapacitors

| Technology type | Supercapacitor | Working voltage (V) | Specific energy (W h $kg^{-1}$) | Power density (W $kg^{-1}$) |
|---|---|---|---|---|
| Electric double-layer | AC//AC | 2.5–3 | 5–7 | 1000–5000 |
| Hybrid | Hard carbon//AC | 2.2–3.8 | 10–30 | 1000–10 000 |
| | AC//$LiMn_2O_4$ | 0.5–1.8 | 5–10 | 100–1000 |
| | $Ni(OH)_2$//AC | 0.5–1.7 | 2–10 | 80–2000 |
| | AC//$PbO_2$ | 0–2 | 10–30 | 50–1000 |
| | AC//$Li_4Ti_5O_{12}$ | 2–3 | 5–20 | 100–1000 |
| | Graphite//AC | 2–3.5 | 5–15 | 100–3000 |

 

#### 5.1.2 X-ray photoelectron spectroscopy (XPS) and Fourier transform infrared (FTIR) spectroscopy

Pseudo-capacitance for supercapacitors mainly depends on the surface faradaic reactions of active electrode materials. Thus, the structure and valence state of surface atoms should be studied. X-ray photoelectron spectroscopy (XPS) can detect the valence state of surface atoms and also the existence of surface functional groups or heteroatoms. Belanger and co-workers used XPS to observe the change in manganese oxidation state, which varied from III to IV for the reduced and oxidized forms of thin film electrodes, respectively, during the charge/discharge process.[166] XPS analysis also showed that $Na^+$ cations from the electrolyte were involved in the charge storage process of $MnO_2$ thin film electrodes. Mullen *et al.* applied XPS technology to detect the existence and relative concentrations of N and B heteroatoms in graphene sheets, confirming homogeneous heteroatom doping in the graphene.[167] Sullivan and his co-operators utilized XPS spectra to detect the formation and reduction of oxygen-containing groups of glassy carbon electrodes after oxidation and reduction.[168] XPS is a very sensitive technique for the detection of functional surface species, as the sampling depth is only about 50 Å. As reported by Sullivan *et al.*,[168] the corresponding XPS results are not relevant for the bulk of the surface layers on the glassy carbon samples. Therefore, FTIR was applied to verify the formation of a surface layer from the differences between the reference spectrum and the spectra of the oxidized, or oxidized and reduced sample.

#### 5.1.3 *In situ* nuclear magnetic resonance (NMR) spectroscopy

Nuclear Magnetic Resonance (NMR) Spectroscopy, a technique that probes local structure and dynamics, can observe individual ionic species independently due to the advantage of element selectivity, and thus can be used to study the charge storage mechanism during the charge/discharge process for a supercapacitor. *Ex situ* NMR involves holding a supercapacitor at a particular voltage, disassembling it, and then acquiring the NMR spectrum of the electrolyte species that remain inside the electrode film. As a contrast, *in situ* NMR allows changes in the local environments of the ions in the electric double layer to be observed for working devices. This approach has provided a qualitative insight into the charging mechanism for a range of supercapacitor systems.[169] Borchardt *et al.*[170] used solid-state $^1H$, $^{11}B$, and $^{13}C$ NMR spectroscopy to investigate the interaction between electrolyte molecules and carbon materials with well-defined porosity. Grey *et al.*[171] applied an *in situ* NMR method to investigate variations at the electrode/electrolyte interface of supercapacitors during charging and discharging (Fig. 14). NMR experiments were carried out at different charging states for a supercapacitor consisting of activated carbon electrodes and an organic electrolyte, which can quantify the number of stored charges. According to the *in situ* NMR measurement results, there exist two distinct charge storage mechanisms: (1) when the voltage of the supercapacitor is below 0.75 V, for the negative electrode, more and more electrolyte anions are desorbed from the carbon micropores, while for the positive electrode, the number of adsorbed anions hardly changes as the voltage increases; (2) when the cell voltage is above 0.75 V, for the positive electrode, the number of adsorbed anions is dramatically increased, while at the negative electrode, anions are continuously desorbed. Recently, Grey and co-workers applied *in situ* NMR to quantify the amount of anions and cations in a working supercapacitor, using microporous carbon as the electrode material.[172] And NMR characterization reveals that the charge storage regime of the positive electrode is different from that of the negative electrode when using $TEABF_4$ in acetonitrile as the electrolyte. For the positive electrode, charging was carried out by the exchange of cations for anions, while cation adsorption dominated at the negative electrode.

### 5.2 Electrochemical profile evaluation

Capacitance (F $g^{-1}$) and energy/power density (W h $kg^{-1}$ and W $kg^{-1}$), tested at a specific current density (A $g^{-1}$), are generally

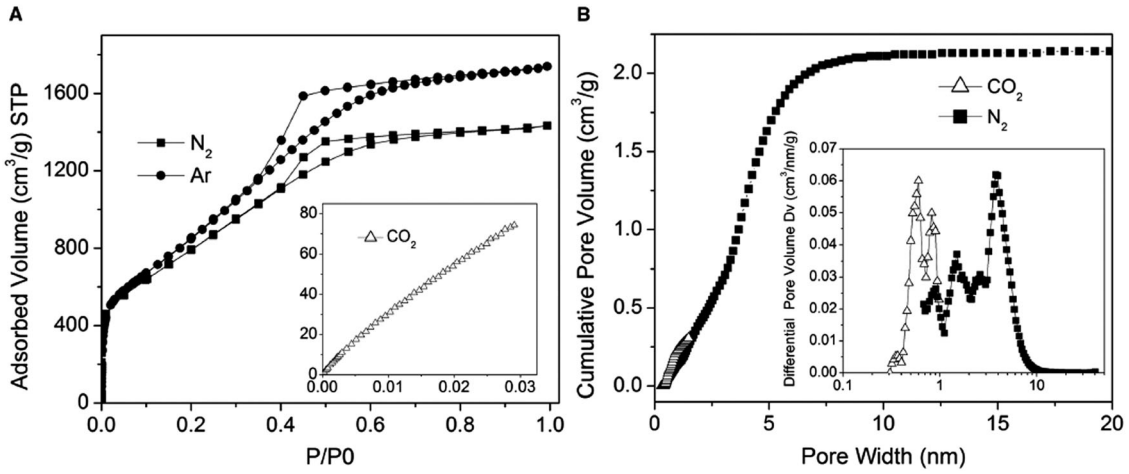


Fig. 13 Gas adsorption/desorption analysis of a-MEGO sample (SSA ~ 3100 $m^2$ $g^{-1}$). (A) High-resolution, low-pressure $N_2$ (77.4 K) and Ar (87.3 K) isotherms (inset is the $CO_2$ (273.2 K) isotherm). (B) Cumulative pore volume and (inset) pore-size distribution for $N_2$ (calculated by using a slit/cylindrical NLDFT model) and $CO_2$ (calculated by using a slit pore NLDFT model). (Reproduced from ref. 58, with permission from the American Association for the Advancement of Science.)

used to evaluate the electrochemical performance of an electrode material or a supercapacitor device. Several typical electrochemical measurements for the evaluation of supercapacitors, such as cyclic voltammetry, galvanostatic charge/discharge, and electrochemical impedance spectroscopy, have been well reviewed in a previous report.[33] Therefore, we only briefly summarize these electrochemical measurements, and clarify some confusion over the evaluation process using these measurements.

**5.2.1 Cyclic voltammetry (CV).** The capacitance of electrode materials can be estimated from the rectangular CV curves using eqn (7):

$$C = i/v \tag{7}$$

Where $C$ is the differential capacitance (F $g^{-1}$), $i$ is the current density (A $g^{-1}$) at mean voltage, and $v$ is the scan rate (V $s^{-1}$). The CV measurement can be directly used to evaluate the average capacitance for an EDLC behaviour and/or a typical pseudocapacitive behaviour that exhibits a rectangular CV curve. However, the faradaic behaviour of a battery-type electrode or the intercalation pseudocapacitive behaviour displays obvious redox peaks in the CV curves, and thus the corresponding average capacitance cannot be directly calculated from CV measurement.

**5.2.2 Galvanostatic discharge/charge (DC) test.** A discharge/charge (DC) test is the most efficient measurement for capacitance evaluation. It is also well known that the capacitance of electrode materials can be calculated on the basis of eqn (8):

$$C = \frac{i \times t}{\Delta V} \tag{8}$$

where $C$ is the capacitance (F $g^{-1}$), $i$ is the current density (A $g^{-1}$), $t$ is the charging/discharging time (s), and $\Delta V$ is the working potential window of the electrode. As mentioned in the mechanism section, the EDLC behaviour exhibits potentially independent charge storage. Therefore, the calculated capacitance of EDLC behaviour does not depend on the choice of working potential window ($\Delta V$). However, for some pseudocapacitive behaviours or intercalation pseudocapacitive behaviours, the capacitances generally centre in specific potential windows. Accordingly, the calculated capacitances of these behaviours vary with the choices of working potential windows.

**5.2.3 Electrochemical impedance spectroscopy (EIS).** EIS measurements are popularly performed by collecting the supercapacitor impedance data at a specific potential, with a small voltage amplitude of 5 or 10 mV over a wide range of frequencies, 0.01 Hz to 100 kHz. The EIS can be expressed as a Nyquist plot composed of three regions, a semicircle at high frequency (larger than $10^4$ Hz), presenting the interface resistance, a high-to-medium frequency region ($10^4$ to 1 Hz), showing the pseudocharge or charge transfer resistance, and a nearly vertical line along the imaginary axis at low frequency (less than 1 Hz), indicating the capacitive behaviour.[173] The relationship between the imaginary part of the impedance $|Z|$ and the frequency $f$ can be obtained from EIS measurements. The capacitance (F) can be calculated using eqn (9):

$$C = \frac{1}{2\pi f|Z|} \tag{9}$$

using a linear portion of a $\log|Z|$ *vs.* $\log f$ curve, which is called the Bode plot. This Bode plot shows that the capacitance decreases with increasing frequency.

**5.2.4 Energy density and power density.** The Ragone plot (energy density *vs.* power density) has been widely employed to evaluate the overall performance of a supercapacitor device. The energy density values of a supercapacitor device can be calculated by numerically integrating the discharge curves:

$$E = \int_{t1}^{t2} IV\,\mathrm{d}t = \frac{1}{2}C(V_1 + V_2)(V_2 - V_1) \tag{10}$$

Where $C$ is the capacitance (F $g^{-1}$) of the supercapacitor, and $V_1$ and $V_2$ are the end-of-charge voltage and the end-of-discharge voltage, respectively. $(V_2 - V_1)$ should be the specific voltage window for the capacitive behaviour of the supercapacitor device. Obviously, only if $V_1$ is zero (0 V), eqn (10) can be re-written as $E = 1/2CV_2^2$. As shown in Fig. 15a, the energy density of an EDLC can be calculated by $E = 1/2CV_2^2$ because its minimum voltage for capacitive behaviour (*i.e.* $V_1$) is 0 V. However, for an

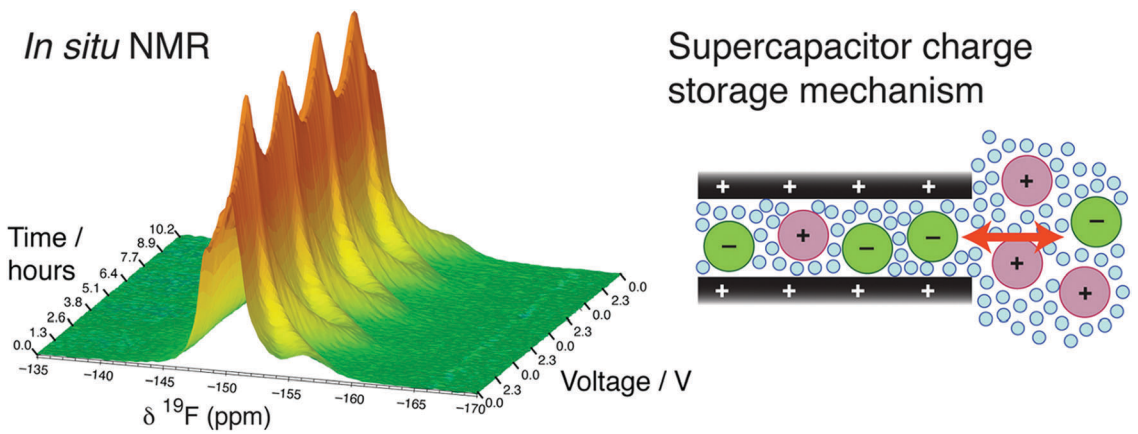


Fig. 14 Successive *in situ* NMR spectra from four full-cyclic voltammetric cycles and charge storage mechanism for supercapacitors. (Reproduced from ref. 171, with permission from the American Chemical Society.)

 

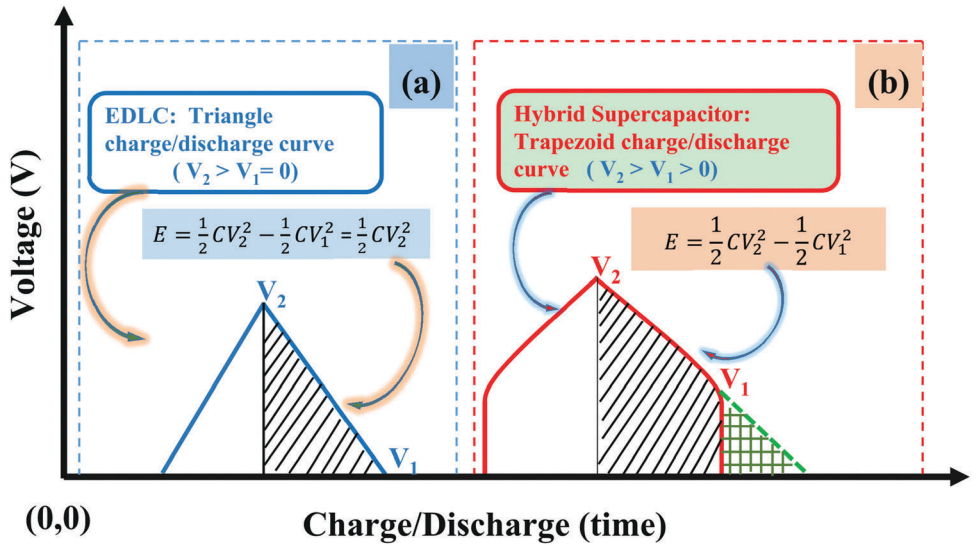


Fig. 15 Schematic of electrochemical profile of EDLC (a) and hybrid supercapacitor (b).

asymmetric supercapacitor or hybrid supercapacitor (see Fig. 15b), the minimum voltage ($V_1$) for capacitive behaviour is higher than 0 V. Therefore, the corresponding energy density can only be calculated using eqn (10).

The power density values of a supercapacitor device can be calculated according to eqn (11):

$$P = \frac{E}{t} \tag{11}$$

Where $P$ is the power density (W kg$^{-1}$), $E$ is the energy density (W h kg$^{-1}$), and $t$ is the discharge time (h).

The maximum power density ($P_m$) for a supercapacitor device can be evaluated using eqn (12):

$$P = \frac{V^2}{4R_s} \tag{12}$$

Where $V$ is the maximum voltage for capacitive behaviour, and $R_s$ is the equivalent series resistance (ESR), which is comprised of the electrode resistance, the electrolyte resistance, and the resistance due to the diffusion of ions in the electrode pores.

It should be noted that the energy/power density (*i.e.* Ragone plot) can only be used to characterize the electrochemical profile of a supercapacitor device, rather than a single electrode. In addition, the energy/power density is critically dependent on the mass loading of electrode-active materials. It is clear that a low mass loading of the electrode always results in a better electrochemical performance, due to its low relative current (A). However, the low mass loading of electrode materials also results in the energy/power density calculated from the mass of active materials being far from that of the practical supercapacitor device. For this point, Gogotsi *et al.* have provided an excellent commentary.[103]

## 6. Application

The opportunities for supercapacitors in a variety of applications are reviewed by Miller *et al.* and Kotz *et al.*[174–176] Recently, the most important application for supercapacitors has been extended to the EV application, including hybrid power with fuel cells or LIBs, as well as pure EC power. Table 3 summarizes

Table 3 Summary of the potential applications of ECs (*i.e.* supercapacitors)

| | Target | Applications | ECs |
|---|---|---|---|
| 1 | Lead–acid battery replacement | Frequent stop & go vehicles<br>• AGV<br>• E-carts<br>Energy backups<br>• Anti-voltage drop<br>• Telco base stations | EDLCs |
| 2 | Regeneration applications | Construction machines<br>Large cranes<br>Elevators | EDLCs |
| 3 | Renewable energies | Storage for PV<br>Load leveling for wind/solar | EDLCsHECs (hybrid ECs) |
| 4 | Vehicles | Hybrid EC/fuel cell EVs & e-bus<br>Hybrid EC/LIB EV & e-bus<br>Short-distance EV bus electric tramcar | EDLCsHECs (hybrid ECs) |

Fig. 16 Trolley bus of Aowei Technology Co., Ltd, based on $Ni(OH)_2$//AC supercapacitor.[177]

the potential applications of ECs. Herein, two examples of EC application in an electric bus (e-bus) are briefly introduced to clarify the future application trend of ECs.

The fast-charge e-bus is one important direction for public city traffic systems. ECs are the most suitable candidate for such applications, as they can be charged within seconds. Aowei Technology Co., Ltd (Shanghai, China) has successfully applied $Ni(OH)_2$//AC hybrid ECs (or hybrid supercapacitors) in a trolley bus (Fig. 16). Its technological parameters are listed in Table 4. This type of trolley bus can be fully charged within a very short time of 90 s and drive 7.9 km at a time with an average and maximum speed of 22 and 44.8 km $h^{-1}$, respectively. It takes 16.5 s to increase the speed from 0 to 40 km $h^{-1}$.

Very recently, EDLCs have been applied in an electric tramcar by the Chinese CSR Co., Ltd (Fig. 17). Table 5 summarizes the properties of the EDLC for the electric tramcar application. This type of electric tramcar can be charged in a very short time of 30 seconds and drive 3–5 kilometres at a time. Without the chemical reactions of a high-capacity supercapacitor, there is no explosion or fire risk, the cycle number can reach 1 million, and its life can be up to 10 years. The characteristics of energy conservation and environmental protection for this type of electric tramcar can alleviate urban traffic pressure and reduce environmental pollution.

Table 4 Technological parameters of trolley bus based on $Ni(OH)_2$/AC supercapacitors

| Working voltage (V) | Max charging voltage (V) | Electrical capacity (F) | Energy storage (W h) | Max charging/ discharging current (A) | Internal impedance (Ω) | Weight (containing box and all types of auxiliary devices) (kg) |
|---|---|---|---|---|---|---|
| 360–600 | 610 | 200 | 6400 | 200 | 0.22 | 980 |


Fig. 17 Electric tramcar of CSR Co., Ltd, based on AC/AC supercapacitor.[178]

Table 5 Properties of AC/AC supercapacitor for electric tramcar application

| Capacity (F) | Model | Maximum ESR (mΩ) | | Leak current (mA) | Weight (kg) | Energy density (W h $kg^{-1}$) | Power density (kW $kg^{-1}$) |
|---|---|---|---|---|---|---|---|
| | | AC@1 kHz | DC | | | | |
| 9500 | NBCSR-9500P-002R7 | ≤0.17 | ≤0.2 | ≤15 | ≤1.34 | 7.15 | 6.78 |

| | |
|---|---|
| Nominal voltage | 2.70 V (DC) |
| Surge voltage | 2.85 V (DC) |
| Operating temperature range | −40 to 65 °C |
| Capacitance tolerance | 0–10% |
| Storage temperature range | −40 to 70 °C |
| Working life at 25 °C | 1 million times or 10 years |

 

# 7. Conclusion

This review summarizes the latest progress with respect to supercapacitors, covering charge storage mechanisms, electrode materials, electrolyte materials, systems, characterization methods, and applications. Porous carbon materials are still widely used electrode materials for supercapacitors. Much research has been devoted to optimizing the pore structure by preparing ordered and hierarchical pores (mesopores and micropores), in order to improve the pore utilization. Doping (*e.g.* N, B) or introducing functional groups has also been employed to improve the specific pseudocapacitance. Carbon nanotubes (CNTs) and reduced graphene oxides (RGO), typically with high electronic conductivity, show promising potential application in flexible and printable supercapacitors. The newly developed intercalation pseudocapacitive materials deliver a high energy density, which normally involves an ion intercalation reaction, but is not controlled by the diffusion process. Nano-sized and nano-structured battery electrode materials have been used for supercapacitors with an enhanced capacitance. An improved understanding of the charge storage mechanisms for battery profiles and capacitive profiles can be acquired from their ion diffusion processes. A hybrid supercapacitor using a battery electrode and a supercapacitor electrode significantly increased the energy density due to both the high cell working voltage and the large capacitance of the battery electrode material in the hybrid system, but led to a decreased power performance, since the power was limited by the rate capability of the battery electrode, in which the charge storage reaction is controlled by ion diffusion. Accordingly, much effort has been devoted to studying the nano-structured material to retain its rate capability. It is still a great challenge to develop supercapacitors with an energy density close to that of current rechargeable batteries (a supercapacitor battery), as well as a high power density and super-long cycle life. However, this may be achieved by using new electrolytes with a voltage window of more than 4 V and wider working temperatures, by discovering new materials that deliver battery capacity with a capacitive profile and low cost, and by developing hybrid devices, as well as by designing advanced electrodes and cells with low resistance. ECs are playing an important role in energy storage and conversion systems. They will either complement batteries, increasing their efficiency and lifetime, or serve as energy solutions, where an extremely long cycling life and fast power delivery are required, especially for fast-charge e-buses and electric tramcars.

# Acknowledgements

This work was partially supported by the National Natural Science Foundation of China (21333002), the State Key Basic Research Program of the People's Republic of China (2011CB935903), and the Shanghai Science & Technology Committee (13JC1407900).

# References

1 M. Armand and J. M. Tarascon, *Nature*, 2008, **451**, 652–657.
2 M. S. Islam and C. A. J. Fisher, *Chem. Soc. Rev.*, 2014, **43**, 185–204.
3 N.-S. Choi, Z. H. Chen, S. A. Freunberger, X. L. Ji, Y. K. Sun, K. Amine, G. Yushin, L. F. Nazar, J. Cho and P. G. Bruce, *Angew. Chem., Int. Ed.*, 2012, **51**, 9994–10024.
4 M. Winter and R. J. Brodd, *Chem. Rev.*, 2004, **104**, 4245–4269.
5 P. Simon and Y. Gogotsi, *Nat. Mater.*, 2008, **7**, 845–854.
6 B. E. Conway, *Electrochemical Supercapacitors: Scientific Fundamentals and Technological Applications*, Kluwer Academic/Plenum Publishers, New York, 1999.
7 B. E. Conway, *J. Electrochem. Soc.*, 1991, **138**, 1539–1548.
8 R. Kötz and M. Carlen, *Electrochim. Acta*, 2000, **45**, 2483–2498.
9 Q. F. Zhang, E. Uchaker, S. L. Candelaria and G. Z. Cuo, *Chem. Soc. Rev.*, 2013, **42**, 3127–3171.
10 P. G. Bruce, B. Scrosati and J.-M. Tarascon, *Angew. Chem., Int. Ed.*, 2008, **47**, 2930–2946.
11 J. M. Tarascon and M. Armand, *Nature*, 2001, **414**, 359–367.
12 X. Y. Lang, A. Hirata, T. Fujita and M. W. Chen, *Nat. Nanotechnol.*, 2011, **6**, 232–236.
13 G. Hu, C. Tang, C. Li, H. Li, Y. Wang and H. Gong, *J. Electrochem. Soc.*, 2011, **158**, A695–A699.
14 H. Wang, H. Yi, X. Chen and X. Wang, *Electrochim. Acta*, 2013, **105**, 353–361.
15 S. G. Kandalkar, J. L. Gunjakar and C. D. Lokhande, *Appl. Surf. Sci.*, 2008, **254**, 5540–5544.
16 B. Senthilkumar, R. K. Selvan, L. Vasylechko and M. Minakshi, *Solid State Sci.*, 2014, **35**, 18–27.
17 M. Zukalová, M. Kalbác, L. Kavan, I. Exnar and M. Graetzel, *Chem. Mater.*, 2005, **17**, 1248–1255.
18 J. Li, Z. L. Tang and Z. T. Zhang, *Chem. Phys. Lett.*, 2006, **418**, 506–510.
19 J. Wang, J. Polleux, J. Lim and B. Dunn, *J. Phys. Chem. C*, 2007, **111**, 14925–14931.
20 Y. G. Wang, Z. S. Hong, M. D. Wei and Y. Y. Xia, *Adv. Funct. Mater.*, 2012, **22**, 5185–5193.
21 K. Brezesinski, J. Wang, J. Haetge, C. Reitz, S. O. Steinmueller, S. H. Tolbert, B. M. Smarsly, B. Dunn and T. Brezesinski, *J. Am. Chem. Soc.*, 2010, **132**, 6982–6990.
22 T. Brezesinski, J. Wang, S. H. Tolbert and B. Dunn, *Nat. Mater.*, 2010, **9**, 146–151.
23 V. Augustyn, J. Come, M. A. Lowe, J. W. Kim, P. L. Taberna, S. H. Tolbert, H. D. Abruna, P. Simon and B. Dunn, *Nat. Mater.*, 2013, **12**, 518–522.
24 M. Sathiya, A. S. Prakash, K. Ramesha, J.-M. Tarascon and A. K. Shukla, *J. Am. Chem. Soc.*, 2011, **133**, 16291–16299.
25 V. Augustyn, P. Simon and B. Dunn, *Energy Environ. Sci.*, 2014, **7**, 1597–1614.
26 T. Brousse, D. Belanger and J. W. Long, *J. Electrochem. Soc.*, 2015, **162**, A5185–A5189.
27 C. Daniel and J. O. Besenhard, *Handbook of battery materials*, Wiley-VCH Verlag GmbH & Co. KGaA, 2nd edn, 2011ch. 5, print-ISBN: 9783527326952, online-ISBN: 9783527637188.
28 H. Lindstrom, S. Sodergren, A. Solbrand, H. Rensmo, J. Hjelm, A. Hagfeldt and S. E. Lindquist, *J. Phys. Chem. B*, 1997, **101**, 7717–7722.
29 A. J. Bard and L. R. Faulkner, *Electrochemical Methods Fundamentals and Applications*, John Wiley, Inc., New York, 2nd edn, 2001, ch. 6, pp. 233, 235.

30 P. Simon, Y. Gogotsi and B. Dunn, *Science*, 2014, **343**, 1210–1211.
31 T. Ogoshi, K. Yoshikoshi, R. Sueto, H. Nishihara and T. Yamagishi, *Angew. Chem., Int. Ed.*, 2015, **54**, 6466–6469.
32 G. P. Wang, L. Zhang and J. J. Zhang, *Chem. Soc. Rev.*, 2012, **41**, 797–828.
33 Z. Yu, L. Tetard, L. Zhai and J. Thomas, *Energy Environ. Sci.*, 2015, **8**, 702–730.
34 E. Frackowiak, *Phys. Chem. Chem. Phys.*, 2007, **9**, 1774–1785.
35 H. J. Liu, J. Wang, C. X. Wang and Y. Y. Xia, *Adv. Energy Mater.*, 2011, **1**, 1101–1108.
36 H. S. Zhou, S. M. Zhu, M. Hibino and I. Honma, *J. Power Sources*, 2003, **122**, 219–223.
37 H. Q. Li, J. Y. Lou, X. F. Zhou, C. Z. Yu and Y. Y. Xia, *J. Electrochem. Soc.*, 2007, **154**, A731–A736.
38 H. Q. Li, R. L. Liu, D. Y. Zhao and Y. Y. Xia, *Carbon*, 2007, **456**, 2628–2635.
39 H. J. Liu, W. J. Cui, L. H. Jin, C. X. Wang and Y. Y. Xia, *J. Mater. Chem.*, 2009, **19**, 3661–3667.
40 H. J. Liu, L. H. Jin, P. He, C. X. Wang and Y. Y. Xia, *Chem. Commun.*, 2009, 6813–6815.
41 H. J. Liu, X. M. Wang, W. J. Cui, Y. Q. Dou, D. Y. Zhao and Y. Y. Xia, *J. Mater. Chem.*, 2010, **20**, 4223–4230.
42 W. Li, F. Zhang, Y. Q. Dou, Z. X. Wu, H. J. Liu, X. F. Qian, D. Gu, Y. Y. Xia and D. Y. Zhao, *Adv. Energy Mater.*, 2011, **1**, 382–386.
43 D. D. Zhou, H. J. Liu, Y. G. Wang, C. X. Wang and Y. Y. Xia, *J. Mater. Chem.*, 2012, **22**, 1937–1943.
44 D. D. Zhou, Y. J. Du, Y. F. Song, Y. G. Wang, C. X. Wang and Y. Y. Xia, *J. Mater. Chem. A*, 2013, **1**, 1192–1200.
45 Y. P. Zhai, Y. Q. Dou, D. Y. Zhao, P. F. Fulvio, R. T. Mayes and S. Dai, *Adv. Mater.*, 2011, **23**, 4828–4850.
46 C. Largeot, C. Portet, J. Chmiola, P. L. Taberna, Y. Gogotsi and P. Simon, *J. Am. Chem. Soc.*, 2008, **130**, 2730–2731.
47 C. O. Ania, V. Khomenko, E. Raymundo-pinero, J. B. Parra and F. Beguin, *Adv. Funct. Mater.*, 2007, **17**, 1828–1836.
48 J. Chmiola, G. Yushin, Y. Gogotsi, C. Portet, P. Simon and P. L. Taberna, *Science*, 2006, **313**, 1760–1763.
49 M. Li, C. Liu, H. Cao, H. Zhao, Y. Zhang and Z. Fan, *J. Mater. Chem. A*, 2014, **2**, 14844–14851.
50 A. B. Fuertes and M. Sevilla, *ACS Appl. Mater. Interfaces*, 2015, **7**, 4344–4353.
51 B. E. Conway, *Electrochemical Supercapacitors*, Kluwer Academic/Plenum Press, New York, 1999.
52 F. Pico, J. M. Rojo, M. L. Sanjuan, A. Anson, A. M. Benito, M. A. Callejas, W. K. Maser and M. T. Martinez, *J. Electrochem. Soc.*, 2004, **151**, A831–A837.
53 E. Frackowiak, S. Gautier, H. Gaucher, S. Bonnamv and F. Beguin, *Carbon*, 1999, **37**, 61–69.
54 E. Frackowiak, S. Depeux, K. Jurewicz, K. Szostak, D. Cazorla-Amoro and F. Beguin, *Chem. Phys. Lett.*, 2002, **361**, 35–41.
55 D. N. Futaba, K. Hata, T. Yamada, T. Hiraoka, Y. Hayamizu, Y. Kakudate, O. Tanaike, H. Hatori, M. Yumura and S. Iijima, *Nat. Mater.*, 2006, **5**, 987–994.
56 N. G. Sahoo, Y. Z. Pan, L. Li and S. H. Chan, *Adv. Mater.*, 2012, **24**, 4203–4210.
57 J. R. Miller, R. A. Outlaw and B. C. Holloway, *Science*, 2010, **329**, 1637–1639.
58 Y. W. Zhu, S. Murarli, M. D. Stoller, K. J. Ganesh, W. W. Cai, P. J. Ferreira, A. Pirkle, R. M. Wallace, K. A. Cychosz, M. Thommes, D. Su, E. A. Stach and R. S. Ruoff, *Science*, 2011, **332**, 1537–1541.
59 K. X. Wang, Y. G. Wang, Y. R. Wang, E. J. Hosono and H. S. Zhou, *J. Phys. Chem. C*, 2009, **113**, 1093–1097.
60 X. F. Qian, Y. Y. Lv, W. Li, Y. Y. Xia and D. Y. Zhao, *J. Mater. Chem.*, 2011, **21**, 13025–13031.
61 R. L. Liu, L. Wan, S. Q. Liu, L. X. Pan, D. Q. Wu and D. Y. Zhao, *Adv. Funct. Mater.*, 2015, **25**, 526–533.
62 X. Q. Yang, D. C. Wu, X. M. Chen and R. W. Fu, *J. Phys. Chem. C*, 2010, **114**, 8581–8586.
63 D. D. Zhou, W. Y. Li, X. L. Dong, Y. G. Wang, C. X. Wang and Y. Y. Xia, *J. Mater. Chem. A*, 2013, **1**, 8488–8496.
64 Y. F. Song, L. Li, Y. G. Wang, C. X. Wang, Z. P. Guo and Y. Y. Xia, *ChemPhysChem*, 2014, **15**, 2084–2093.
65 Y. F. Song, S. Hu, X. L. Dong, Y. G. Wang, C. X. Wang and Y. Y. Xia, *Electrochim. Acta*, 2014, **146**, 485–494.
66 F. Su, C. K. Poh, J. S. Chen, G. Xu, D. Wang, Q. Li, J. Lin and X. W. Lou, *Energy Environ. Sci.*, 2011, **4**, 717–724.
67 D. Hulicova-Jurcakova, M. Seredych, G. Q. Lu and T. J. Bandosz, *Adv. Funct. Mater.*, 2009, **19**, 438–447.
68 Y. F. Zhao, W. Ran, J. He, Y. F. Song, C. M. Zhang, D. B. Xiong, F. Gao, J. S. Wu and Y. Y. Xia, *ACS Appl. Mater. Interfaces*, 2015, **7**, 1132–1139.
69 Y. Li, C. X. Lu, S. C. Zhang, F. Y. Su, W. Z. Shen, P. Zhou and C. L. Ma, *J. Mater. Chem. A*, 2015, **3**, 14817–14825.
70 Y. S. Yun, S. Y. Cho, J. Y. Shim, B. H. Kim, S. J. Chang, S. J. Baek, Y. S. Huh, Y. Tak, Y. W. Park, S. J. Park and H. J. Jin, *Adv. Mater.*, 2013, **25**, 1993–1998.
71 M. Wahid, G. Parte, D. Phase and S. Ogale, *J. Mater. Chem. A*, 2015, **3**, 1208–1215.
72 X. L. Wu, L. L. Jiang, C. L. Long and Z. J. Fan, *Nano Energy*, 2015, **13**, 527–536.
73 Z. J. Li, W. Lv, C. Zhang, B. H. Li, F. Y. Kang and Q. H. Yang, *Carbon*, 2015, **92**, 11–14.
74 H. Choi and H. Yoon, *Nanomaterials*, 2015, **5**, 906–936.
75 S. Faraji and F. N. Ani, *J. Power Sources*, 2014, **263**, 338–360.
76 J. P. Zheng and T. R. Jow, *J. Electrochem. Soc.*, 1995, **142**, L6–L8.
77 T. R. Jow and J. P. Zheng, *J. Electrochem. Soc.*, 1998, **145**, 49–52.
78 W. Sugimoto, H. Iwata, Y. Yasunaga, Y. Murakami and Y. Takasu, *Angew. Chem., Int. Ed.*, 2003, **42**, 4092–4096.
79 J. P. Zheng and T. R. Jow, *J. Power Sources*, 1996, **62**, 155–159.
80 J. P. Zheng, *Electrochem. Solid-State Lett.*, 1999, **2**, 359–361.
81 Q. L. Fang, D. A. Evans, S. L. Roberson and J. P. Zheng, *J. Electrochem. Soc.*, 2001, **148**, A833–A837.
82 Y. U. Jeong and A. Manthiram, *Electrochem. Solid-State Lett.*, 2000, **3**, 205–208.
83 Y. U. Jeong and A. Manthiram, *J. Electrochem. Soc.*, 2001, **148**, A189–A193.
84 C. C. Hu and Y. H. Huang, *Electrochim. Acta*, 2001, **46**, 3431–3444.

 

85 C. C. Hu, W. C. Chen and K. H. Chang, *J. Electrochem. Soc.*, 2004, **151**, A281–A290.
86 N. Wu, S. Kuo and M. Lee, *J. Power Sources*, 2002, **104**, 62–65.
87 S. Trasatti, *Electrochim. Acta*, 1991, **36**, 225–241.
88 W. Sugimoto, T. Shibutani, Y. Murakami and Y. Takasu, *Electrochem. Solid-State Lett.*, 2002, **5**, A170–A172.
89 Y. Takasu and Y. Murakami, *Electrochim. Acta*, 2000, **45**, 4135–4141.
90 W. Wei, X. Cui, W. Chen and D. G. Ivey, *Chem. Soc. Rev.*, 2011, **40**, 1697–1721.
91 M. Toupin, T. Brousse and D. Belanger, *Chem. Mater.*, 2004, **16**, 3184–3190.
92 H. Jiang, T. Zhao, J. Ma, C. Yan and C. Li, *Chem. Commun.*, 2011, **47**, 1264–1266.
93 J. Zhu, W. Shi, N. Xiao, X. Rui, H. Tan, X. Lu, H. H. Hng, J. Ma and Q. Yan, *ACS Appl. Mater. Interfaces*, 2012, **4**, 2769–2774.
94 H. Jiang, T. Sun, C. Li and J. Ma, *J. Mater. Chem.*, 2012, **22**, 2751–2756.
95 J. Y. Luo and Y. Y. Xia, *J. Electrochem. Soc.*, 2007, **154**, A987–A992.
96 Z. S. Wu, W. C. Ren, D. W. Wang, F. Li, B. Liu and H. M. Cheng, *ACS Nano*, 2010, **10**, 5835–5842.
97 W. Chen, R. B. Rakhi, L. B. Hu, X. Xie, Y. Cui and H. N. Alshareef, *Nano Lett.*, 2011, **11**, 5165–5172.
98 Y. Guo, J. Li, M. D. Chen and G. Z. Gao, *J. Power Sources*, 2015, **273**, 804–809.
99 Y. J. Wu, G. H. Gao and G. M. Wu, *J. Mater. Chem. A*, 2015, **3**, 1828–1832.
100 T. Y. Wei, C. H. Chen, H. C. Chien, S. Y. Lu and C. C. Hu, *Adv. Mater.*, 2010, **22**, 347–351.
101 A. R. Armstrong, G. Armstrong, J. Ganales and P. G. Bruce, *J. Power Sources*, 2005, **146**, 501–506.
102 H. B. Li, M. H. Yu, F. X. Wang, P. Liu, Y. Liang, J. Xiao, C. X. Wang, Y. X. Tong and G. W. Yang, *Nat. Commun.*, 2013, **4**, 1894.
103 Y. Gogotsi and P. Simon, *Science*, 2011, **334**, 917–918.
104 H. Jiang, T. Zhao, C. Z. Li and J. Ma, *J. Mater. Chem.*, 2011, **21**, 3818–3823.
105 Y. F. Yuan, X. H. Xia, J. B. Wu, J. L. Yang, Y. B. Chen and S. Y. Guo, *Electrochim. Acta*, 2011, **56**, 2627–2632.
106 U. M. Patil, K. V. Gurav, V. J. Fulari, C. D. Lokhande and O. S. Joo, *J. Power Sources*, 2009, **188**, 338–342.
107 G. W. Yang, C. L. Xu and H. L. Li, *Chem. Commun.*, 2008, 6537–6539.
108 H. L. Wang, S. Gasalongue, Y. Y. Liang and H. J. Dai, *J. Am. Chem. Soc.*, 2010, **132**, 7472–7477.
109 J. W. Lee, T. B. Ahn, D. Soundararajan, J. M. Ko and J. D. Kim, *Chem. Commun.*, 2011, **47**, 6305–6307.
110 Y. G. Wang, L. Yu and Y. Y. Xia, *J. Electrochem. Soc.*, 2006, **153**, A743–A748.
111 Y. G. Wang, D. D. Zhou, D. Zhao, M. Y. Hou, C. X. Wang and Y. Y. Xia, *J. Electrochem. Soc.*, 2013, **160**, A98–A104.
112 B. Kang and G. Ceder, *Nature*, 2009, **458**, 190–193.
113 Y. G. Wang, D. Zhao, R. C. Che and Y. Y. Xia, *J. Power Sources*, 2013, **236**, 230–237.
114 H. T. Guo, W. N. He, Y. Lu and X. T. Zhang, *Carbon*, 2015, **92**, 133–141.
115 Y. Huang, J. Y. Tao, W. J. Meng, M. S. Zhu, Y. Huang, Y. Q. Fu, Y. H. Gao and C. Y. Zhi, *Nano Energy*, 2015, **11**, 518–525.
116 L. Wang, X. Feng, L. T. Ren, Q. H. Piao, J. Q. Zhong, Y. B. Wang, H. W. Li, Y. F. Chen and B. Wang, *J. Am. Chem. Soc.*, 2015, **137**, 4920–4923.
117 Y. F. Zhao, Z. Zhang, Y. Q. Ren, W. Ran, X. Q. Chen, J. S. Wu and F. Gao, *J. Power Sources*, 2015, **286**, 1–9.
118 Y. Liu, Y. Ma, S. Y. Guang, H. Y. Xu and X. Y. Su, *J. Mater. Chem. A*, 2014, **2**, 813–823.
119 Z. H. Wang, P. Tammela, M. Stromme and L. Nyholm, *Nanoscale*, 2015, **7**, 3418–3423.
120 P. J. Hung, K. H. Chang, Y. F. Lee, C. C. Hu and K. M. Lin, *Electrochim. Acta*, 2010, **55**, 6015–6021.
121 N. Jung, S. Kwon, D. Lee, D. M. Yoon, Y. M. Park, A. Benayad, J. Y. Choiand and J. S. Park, *Adv. Mater.*, 2013, **25**, 6854–6858.
122 C. Zhong, Y. Deng, W. Hu, J. Qiao, L. Zhang and J. J. Zhang, *Chem. Soc. Rev.*, 2015, **44**, 7484–7539.
123 C. Wolff, S. Jeong, E. Paillard, A. Balducci and S. Passerini, *J. Power Sources*, 2015, **293**, 65–70.
124 C. Kong, W. Qian, C. Zheng, Y. Yu, C. Cui and F. Wei, *Chem. Commun.*, 2013, **49**, 10727–10729.
125 H. J. Fei, C. Y. Yang, H. Bao and G. C. Wang, *J. Power Sources*, 2014, **266**, 488–495.
126 Q. Chen, X. M. Li, X. B. Zang, Y. C. Cao, Y. J. He, P. X. Li, K. L. Wang, J. Q. Wei, D. H. Wu and H. W. Zhu, *RSC Adv.*, 2014, **4**, 36253–36256.
127 C. Huang and P. S. Grant, *Sci. Rep.*, 2013, **3**, 2393.
128 M. Gnerlich, H. B. Yoav, J. N. Culver and D. R. Ketchum, *J. Power Sources*, 2015, **293**, 649–656.
129 L. H. Su, X. G. Zhang, C. H. Mi, B. Gao and Y. Liu, *Phys. Chem. Chem. Phys.*, 2009, **11**, 2195–2202.
130 L. Q. Mai, A. Minhas-Khan, X. Tian, K. M. Hercule, Y. L. Zhao, X. Lin and X. Xu, *Nat. Commun.*, 2009, **4**, 2923.
131 A. Burke, *Electrochim. Acta*, 2007, **53**, 1083–1091.
132 L. Demarconnay, E. R. Pinero and F. Beguin, *Electrochem. Commun.*, 2010, **12**, 1275–1278.
133 Q. Gao, L. Demarconnay, E. R. Pinero and F. Beguin, *Energy Environ. Sci.*, 2012, **5**, 9611–9617.
134 T. H. Wu, C. T. Hsu, C. C. Hu and L. J. Hardwick, *J. Power Sources*, 2013, **242**, 289–298.
135 H. Xia, Y. S. Meng, G. L. Yuan, C. Cui and L. Lu, *Electrochem. Solid-State Lett.*, 2012, **15**, A60–A63.
136 G. Ma, D. Y. Guo, K. Sun, H. Peng, Q. Yang, X. Z. Zhou, X. L. Zhao and Z. Q. Lei, *RSC Adv.*, 2015, **5**, 64704–64710.
137 S. Shivakumara, B. Kishore, T. R. Penki and N. Munichandraiah, *Solid State Commun.*, 2014, **199**, 26–32.
138 T. Brousse, M. Toupin and D. Belanger, *J. Electrochem. Soc.*, 2004, **151**, A614–A622.
139 Q. Qu, P. Zhang, B. Wang, Y. H. Chen, S. Tian, Y. P. Wu and R. Holze, *J. Phys. Chem. C*, 2009, **113**, 14020–14027.
140 J. W. Long, D. Belanger, T. Brousse, W. Sugimoto, M. B. Sassin and O. Crosnier, *MRS Bull.*, 2011, **36**, 513–522.
141 T. M. Ou, C. T. Hsu and C. C. Hu, *J. Electrochem. Soc.*, 2015, **162**, A5124–A5132.

142 L. Li, S. Peng, H. B. Wu, L. Yu, S. Madhavi and X. W. Lou, *Adv. Energy Mater.*, 2015, **5**, 1500753.
143 S. Peng, L. Li, H. B. Wu, S. Madhavi and X. W. Lou, *Adv. Energy Mater.*, 2015, **5**, 1401172.
144 J. Liu, L. Zhang, H. B. Wu, J. Lin, Z. Shen and X. W. Lou, *Energy Environ. Sci.*, 2014, **7**, 3709–3719.
145 M. Rajkumar, C. T. Hsu, T. H. Wu, M. G. Chen and C. C. Hu, *Prog. Nat. Sci.: Mater. Int.*, 2015, **25**, 527–544.
146 F. X. Ma, L. Yu, C. Y. Xu and X. W. Lou, *Energy Environ. Sci.*, 2016, **9**, 862–866.
147 X. Y. Yu, L. Yu and X. W. Lou, *Adv. Energy Mater.*, 2016, **6**, 1501333.
148 L. Yu, B. Guan, W. Xiao and X. W. Lou, *Adv. Energy Mater.*, 2015, **5**, 1500981.
149 Y. Guo, L. Yu, C. Y. Wang, Z. Lin and X. W. Lou, *Adv. Funct. Mater.*, 2015, **25**, 5184–5189.
150 Y. M. Chen, Z. Li and X. W. Lou, *Angew. Chem., Int. Ed.*, 2015, **54**, 10521–10524.
151 C. M. Zhang, L. J. Xie, W. Song, J. L. Wang, G. H. Sun and K. X. Li, *J. Electroanal. Chem.*, 2013, **706**, 1–6.
152 J. L. Yin and J. Y. Park, *J. Solid State Electrochem.*, 2015, **19**, 2391–2398.
153 N. F. Yu and L. J. Gao, *Electrochem. Commun.*, 2009, **11**, 220–222.
154 P. Perret, Z. Khani, T. Brousse, D. Belanger and D. Guay, *Electrochim. Acta*, 2011, **56**, 8122–8128.
155 J. H. Park, O. O. Park, K. H. Shin, C. S. Jin and J. H. Kim, *Electrochem. Solid-State Lett.*, 2002, **5**, H7–H10.
156 G. G. Amatucci, F. Badway, A. D. Pasquier and T. Zheng, *J. Electrochem. Soc.*, 2001, **148**, A930–A939.
157 A. D. Pasquier, I. Plitz, J. Gural and S. Menocal, *J. Power Sources*, 2003, **113**, 62–71.
158 L. Cheng, H. J. Liu, J. J. Zhang, H. M. Xiong and Y. Y. Xia, *J. Electrochem. Soc.*, 2006, **153**, A1472–A1477.
159 J. J. Yang, C. H. Choi, H. B. Seo, H. J. Kim and S. G. Park, *Electrochim. Acta*, 2012, **86**, 277–281.
160 V. Khomenko, E. R. Pinero and F. Beguin, *J. Power Sources*, 2008, **177**, 643–651.
161 S. W. Li and X. H. Wang, *J. Power Sources*, 2015, **282**, 394–400.
162 H. Y. Wang and M. Yoshio, *Electrochem. Commun.*, 2006, **8**, 1481–1486.
163 Y. G. Wang and Y. Y. Xia, *Electrochem. Commun.*, 2005, **7**, 1138–1142.
164 D. Cericola, P. Novak, A. Wokaun and R. Kotz, *Electrochim. Acta*, 2011, **56**, 8403–8411.
165 Y. K. Kwon, W. C. Choi, H. S. Choi and J. K. Lee, *Electron. Mater. Lett.*, 2013, **9**, 751–754.
166 M. Toupin, T. Brousse and D. Belanger, *Chem. Mater.*, 2004, **16**, 3184–3190.
167 Z. S. Wu, A. Winter, L. Chen, Y. Sun, A. Turchanin, X. L. Feng and K. Mullen, *Adv. Mater.*, 2012, **24**, 5130–5135.
168 M. G. Sullivan, B. Schnyder, M. Bartsch, D. Alliata, C. Barbero, R. Imhof and R. Kotz, *J. Electrochem. Soc.*, 2000, **147**, 2636–2643.
169 F. Blanc, M. Leskes and C. P. Grey, *Acc. Chem. Res.*, 2013, **46**, 1952–1963.
170 L. Borchardt, M. Oschatz, S. Paasch, S. Kaskel and E. Brunner, *Phys. Chem. Chem. Phys.*, 2013, **15**, 15177–15184.
171 H. Wang, A. C. Forse, J. M. Griffin, N. M. Trease, L. Trognko, P. L. Taberna, P. Simon and C. P. Grey, *J. Am. Chem. Soc.*, 2013, **135**, 18968–18980.
172 J. M. Griffin, A. C. Forse, W. Y. Tsai, P. L. Taberna, P. Simon and C. P. Grey, *Nat. Mater.*, 2015, **14**, 812–819.
173 W. Sun, R. L. Zheng and X. Y. Chen, *J. Power Sources*, 2010, **195**, 7120–7125.
174 J. R. Miller and P. Simon, *Science*, 2008, **321**, 651–652.
175 R. Kotz and M. Carlen, *Electrochim. Acta*, 2000, **45**, 2483–2498.
176 J. R. Miller and A. F. Burke, *Electrochem. Soc. Interface*, 2008, **17**, 53–57.
177 http://www.aowei.com/case_view.php?typeid=1&id=4.
178 http://baike.baidu.com/link?url=IzlpZIawcdNNLxZkFDOCUN-JrQYwPs_e0Quh23s90Hd8aGeTm4oahoouno-LxzCdRfWj0-Ao0tQnmqLbrXSZ6dMK.

 